HHS Public Access

Author manuscript

Acta Biomater. Author manuscript; available in PMC 2024 October 07.

Published in final edited form as:

Acta Biomater. 2024 March 15; 177: 278–299. doi:10.1016/j.actbio.2024.01.040.

Mechanical, structural, and physiologic differences between above and below-knee human arteries

Pauline Struczewska[a,1], **Sayed Ahmadreza Razian**[a,1], **Kaylee Townsend**[b], **Majid Jadidi**[a], **Ramin Shahbad**[a], **Elham Zamani**[a], **Jennifer Gamache**[c], **Jason MacTaggart**[c], **Alexey Kamenskiy**[a,*]

[a]Department of Biomechanics, University of Nebraska Omaha, Omaha, NE, USA

[b]Live On Nebraska, Omaha, NE, USA

[c]Department of Surgery, University of Nebraska Medical Center, Omaha, NE, USA

Abstract

Peripheral Artery Disease (PAD) affects the lower extremities and frequently results in poor clinical outcomes, especially in the vessels below the knee. Understanding the biomechanical and structural characteristics of these arteries is important for improving treatment efficacy, but mechanical and structural data on tibial vessels remain limited. We compared the superficial femoral (SFA) and popliteal (PA) arteries that comprise the above-knee femoropopliteal (FPA) segment to the infrapopliteal (IPA) anterior tibial (AT), posterior tibial (PT), and fibular (FA) arteries from the same 15 human subjects (average age 52, range 42–67 years, 87 % male). Vessels were imaged using μCT, evaluated with biaxial mechanical testing and constitutive modeling, and assessed for elastin, collagen, smooth muscle cells (SMCs), and glycosaminoglycans (GAGs). IPAs were more often diseased or calcified compared to the FPAs. They were also twice smaller, 53 % thinner, and significantly stiffer than the FPA longitudinally, but not circumferentially. IPAs experienced 48 % higher physiologic longitudinal stresses (62 kPa) but 27 % lower circumferential stresses (24 kPa) and similar cardiac cycle stretch of <1.02 compared to the FPA. IPAs had lower longitudinal pre-stretch (1.12) than the FPAs (1.29), but there were no differences in the stored elastic energy during pulsation. The physiologic circumferential stiffness was similar in the above and below-knee arteries (718 kPa vs 754 kPa). Structurally, IPAs had less elastin, collagen, and GAGs than the FPA, but maintained similar SMC content. Our findings contribute to a better understanding of segment-specific human lower extremity artery biomechanics and may inform the development of better medical devices for PAD treatment.

[*]Corresponding author at: Department of Biomechanics, Biomechanics Research Building, University of Nebraska at Omaha, USA. akamenskiy@unomaha.edu (A. Kamenskiy).

[1]Both authors acknowledge equal contributions for co-first authorship for this work

Declaration of competing interest

The authors declare that they have no known competing financial interests or personal relationships that could have appeared to influence the work reported in this paper.

Disclosures

The authors have no relevant disclosures.

Keywords

Femoropopliteal artery; Infrapopliteal arteries; Tibial arteries; Mechanical properties; Structural characteristics

1. Introduction

Peripheral Artery Disease (PAD) often refers to the atherosclerotic obstruction of the femoropopliteal (FPA) or infrapopliteal (IPA) arteries in the lower extremities. It affects over 150 million people worldwide and is associated with high morbidity, mortality, and quality of life impairment [1]. The FPA starts as a superficial femoral artery (SFA) and becomes the popliteal artery (PA) as it traverses the adductor hiatus, a gap between the adductor magnus muscle and the femur. It then passes from the anterior thigh posteriorly into the popliteal fossa behind the knee. Below the knee, the PA branches into the anterior tibial (AT), posterior tibial (PT), and fibular (peroneal) arteries (FA) (Fig. 1). The two main sites of FPA obstructions are in the PA at the adductor hiatus and behind the knee [2], and the primary mechanism of the restrictive lesions is atherosclerosis [3]. Obstructions in the IPA are 4-fold more common than in the FPA, but the underlying mechanism is thrombosis or thromboembolism, with 68 % of severely stenosed IPAs not having significant atherosclerosis [3].

The total annual costs of hospitalizations for patients with PAD exceed $21 billion per year, and per-patient PAD expenses are higher than those for both coronary artery disease and cerebrovascular disease [4,5]. The high cost of PAD is mainly attributed to the high number of peripheral vascular operations and interventions that fail, resulting in poor clinical outcomes and a frequent need for repeat repairs [6–12]. Results are particularly poor below the knee. The primary patency of autogenous vein and synthetic bypass grafts at 1 year is 61 % [7] and 42–55 % [13], respectively. At 2 years, it reduces to 31–41 %, at 3 years to 21–32 % [13], and at 5 years to 16–23 % [13,14]. The results of endovascular repairs are equally disappointing, with the 1-year 53–69 % primary patency of IPA angioplasty [15–17], despite technical success rates of >90 % [18].

Biomechanical and structural characteristics of arteries play important roles in vascular mechanobiology [19] and define the interactions with repair devices and materials. An understanding of segmental differences between the above and below-knee arteries can help explain the discrepancy in disease patterns and help improve treatments through location-specific designs, but structural, mechanical, and physiologic characteristics of human AT, PT, and FAs have not been comprehensively investigated, let alone compared with the SFA and PA. The goal of our study was to compare these characteristics in the same human subjects using high-resolution imaging, biaxial mechanical testing, structural analysis with bidirectional histology, and constitutive modeling. The presented data provide a better understanding of the differences in FPA and IPA biomechanics and mechanophysiology that can aid in the development of improved devices and materials for PAD treatment.

2. Methods

2.1. Arterial specimens

Arteries were procured by Live On Nebraska from $N = 15$ human subjects (average age 52 years old, range 42–67 years, 87 % male) within 24 h of death after obtaining consent from the next of kin to use tissues for research. All procedures adhered to the ethical standards set forth by the 1964 Helsinki Declaration and its subsequent updates, and all necessary steps were taken to protect the confidentiality and anonymity of the donors. Table 1 summarizes the details of subject demographics and risk factors, along with their cause of death and the degree of vascular pathology [20,21]. Specimens extended from the take off of the profunda femoris artery to the tibial vessels and included the superficial femoral (SFA) and popliteal arteries (PA) that made up the FPA, and the infrapopliteal (IPA) anterior tibial (AT), posterior tibial (PT) and fibular (peroneal) arteries (FA) below the knee. All vessels were dissected from the surrounding tissues, and branches were ligated using a surgical 5–0 suture and medium-sized Weck Hem-o-Lok polymer ligation clips.

2.2. Imaging

The FPA and the IPA vessels were attached to custom-made fixtures, covered with plastic wrap to prevent dehydration, and pressurized to ~80 mmHg using shaving foam to open the lumen. Shaving foam was used because its attenuation coefficient allows it to be invisible on X-ray. The arteries were imaged using μCT Easy-TomS system (RX solutions, Chavanod, France) to assess the degree of vascular calcification. Scanning was done at 100 kV and 350 μA, the frame rate was set to 10, and the number of frames to 4. A 0.35 mm copper filter was used to prevent artifacts caused by calcification. The arteries were imaged at 80–94 μm resolution, and the scans took 34–51 min, which was a good compromise between resolution and scanning time that allowed to avoid specimen dehydration. The rotational raw TIFF images were converted to cross-sectional bitmaps and reconstructed using RX (RX solutions, Chavanod, France) software. Cross-sectional bitmap images were then exported from RX and stitched together in Materialise Mimics v25 (Materialise NV, Leuven, Belgium), forming 3D models. Soft tissue and calcification were reconstructed separately, and the volume of calcium in each analyzed arterial segment was recorded relative to the volume of that segment.

2.3. Morphometry measurements

After μCT imaging, arteries were flushed with 0.9 % phosphate-buffered saline (PBS) to remove foam residues and cut for morphometry measurements and planar biaxial mechanical testing. Morphometry measurements included inner diameter, wall thickness of the load-free (no internal pressure) and stress-free (radially-cut) arterial rings, a circumferential opening angle of the radially-cut ring, and a longitudinal opening angle of axial strips obtained from the segments adjacent to the biaxial test (please refer to Fig. 9 of the Appendix or to Jadidi et al. [23] or Kamenskiy et al. [24]). All measurements were done using photographs after the tissue had at least 30 min to relax in a petri dish filled with PBS.

2.4. Biaxial mechanical testing

Mechanical testing of the SFA, PA, AT, PT, FA, and the transition zones (the tibioperoneal trunk (TPT) between the AT and the PT/FA and the arch of the AT) was done in 0.9 % PBS at 37 °C using a CellScale Biotester (Waterloo, ON, Canada) equipped with 2.5 N loadcells. SFA specimens were taken approximately 3–5 cm from the profunda femoris artery, PA specimens were obtained 2–3 cm proximal to the TPT, and below-knee AT, PT, and FA were taken 1–2 cm distal to their take-off. We have also analyzed segments of the AT arch and the TPT as transition zones between the vessels. For each donor, arterial segments were tested in random order to eliminate bias. The experiments were stretch-controlled, and the test axes were aligned with the longitudinal and circumferential directions of the artery [21,23,24]. The specimens varied in size depending on arterial diameter, and the arteries were attached to the device using biorakes because our previous analysis demonstrated minimal shear [25]. The intimal surface of the specimens faced upward and was sprinkled with graphite markers to allow measurements of the deformation gradient.

Because the tests were stretch-controlled, we first estimated the maximum stretch limits for each specimen such that the tests captured the non-linearity in the stress-stretch response while also staying within the elastic domain, i.e., avoiding damage and permanent set effects. We have established these thresholds for different age groups previously [26], and for the FPAs aged 39 to 49 years old have used stretches corresponding to a maximum force of 800 mN. Older arteries experience damage at lower thresholds [26], and we have thus used a maximum of 500 mN for 50 to 70 year-old FPA specimens. The same 500 mN threshold was used for all IPA vessels because they were thinner and easier to damage.

The main test sequence included 10 preconditioning cycles to the maximum stretches, followed by 21 multi-ratio stretch-controlled protocols ranging from 1:0.1 to 1:0.9 and from 0.9:1 to 0.1:1 with a step of 0.1 at 0.01 s^{-1} strain rate. Three equibiaxial 1:1 stability checks were used at the beginning, middle, and at the end of the testing sequence to ensure that the specimens did not accumulate damage.

2.5. Constitutive modeling

The stress-stretch experimental data from all multi-ratio experimental protocols were used to determine the constitutive parameters for the four-fiber-family invariant-based constitutive model that has previously been shown to describe the behavior of human FPAs in all ages very well [20,21,23–25,27,28]. Briefly, the strain energy function includes passive contributions from the ground matrix consisting of proteoglycans, glycosaminoglycans, and other constituents modeled as a neo-Hookean material, longitudinally-oriented elastic fibers, circumferential smooth muscle cells (SMCs), and two families of collagen fibers. This strain energy function has eight constitutive parameters and the form:

$$W = W_{gr} + W_{el} + W_{smc} + W_{col1} + W_{col2} \quad (1)$$

$$W_{gr} = \frac{C_{gr}}{2}(I_{\mathbf{C}} - 3) \tag{2}$$

$$W_{el} = \frac{C_1^{el}}{4C_2^{el}}\left(e^{C_2^{el}\langle I_4^{el} - 1\rangle^2} - 1\right) \tag{3}$$

$$W_{smc} = \frac{C_1^{smc}}{4C_2^{smc}}\left(e^{C_2^{smc}\langle I_4^{smc} - 1\rangle^2} - 1\right) \tag{4}$$

$$W_{col,j} = \frac{C_1^{col}}{4C_2^{col}}\left(e^{C_2^{col}\langle I_4^{col,j} - 1\rangle^2} - 1\right), \quad j = 1, 2 \tag{5}$$

Where the invariants of the right Cauchy-Green stretch tensor $\mathbf{C} = \mathbf{F}^T\mathbf{F}$ are:

$$I_{\mathbf{C}} = tr(\mathbf{C}) = \lambda_r^2 + \lambda_\theta^2 + \lambda_z^2 \tag{6}$$

$$I_4^{col,1} = I_4^{col,2} = I_4^{col} = \lambda_z^2 cos^2\gamma + \lambda_\theta^2 sin^2\gamma \tag{7}$$

$$I_4^{el} = \lambda_z^2 \tag{8}$$

$$I_4^{smc} = \lambda_\theta^2 \tag{9}$$

Here $\lambda_z, \lambda_\theta$ are longitudinal and circumferential stretches, and a fiber family i forms an angle γ^i with the longitudinal direction so that $\gamma^i = 0°$ aligns the fibers longitudinally with material parameters C_1^{el}, C_2^{el} (elastin), $\gamma^i = 90°$ corresponds to the circumferential alignment with material parameters C_1^{smc}, C_2^{smc} (SMCs), and the two families of helical collagen fibers at the angle $\gamma^i = \gamma$ to the longitudinal direction with mechanically equivalent contributions

and parameters C_1^{col}, C_2^{col} (collagen). Macaulay brackets $\left\langle (\cdot) \right\rangle = \frac{1}{2}[(\cdot) + |(\cdot)|]$ are used to filter positive values, so the constituents only contribute to stress during tension.

Assuming incompressibility [29], the Cauchy stresses in the longitudinal (z) and circumferential (θ) directions can be expressed as (for details, please refer to Jadidi et al. [21,30]):

$$t_{\theta\theta} = C_g\lambda_\theta^2 + C_1^{smc}\left\langle \lambda_\theta^2 - 1 \right\rangle e^{C_2^{smc}(\lambda_\theta^2 - 1)^2}\lambda_\theta^2 + 2C_1^{col}\left\langle I_4^{col} - 1 \right\rangle e^{C_2^{col}(I_4^{col} - 1)^2}\lambda_\theta^2 sin^2\gamma \tag{10}$$

$$t_{zz} = C_g\lambda_z^2 + C_1^{el}\left\langle \lambda_z^2 - 1 \right\rangle e^{C_2^{el}(\lambda_z^2 - 1)^2}\lambda_z^2 + 2C_1^{col}\left\langle I_4^{col} - 1 \right\rangle e^{C_2^{col}(I_4^{col} - 1)^2}\lambda_z^2 cos^2\gamma \tag{11}$$

The eight constitutive parameters for each specimen were determined using the Differential Evolution algorithm [31] by minimizing the Objective Function based on the Root Mean Square Error (RMSE) between the experimental and the theoretically calculated stresses:

$$RMSE = \sqrt{\frac{1}{2n}\sum_1^n \left(t_{zz}^{exp,i} - t_{zz}^{th,i}\right)^2 + \left(t_{\theta\theta}^{exp,i} - t_{\theta\theta}^{th,i}\right)^2} \tag{12}$$

where $\mathbf{t}^{\exp}$ is the experimental Cauchy stress and $\mathbf{t}^{th}$ is the theoretically calculated Cauchy stress, n is the number of experimental data points across all test protocols.

The coefficient of determination R^2 was used to assess the quality of the models' fit to the experimental data:

$$R_\theta^2 = 1 - \frac{\sum_i^n \left(t_{\theta\theta}^{exp,i} - t_{\theta\theta}^{th,i}\right)}{\sum_i^n \left(t_{\theta\theta}^{exp,i} - t_{\theta\theta}^{exp,avg}\right)} \tag{13}$$

$$R_z^2 = 1 - \frac{\sum_i^n \left(t_{zz}^{exp,i} - t_{zz}^{th,i}\right)}{\sum_i^n \left(t_{zz}^{exp,i} - t_{zz}^{exp,avg}\right)} \tag{14}$$

$$R^2 = \frac{R_\theta^2 + R_z^2}{2}. \tag{15}$$

Due to the inherent interconnectedness and potential non-uniqueness of material parameters, averaging them to acquire the stress-stretch response of an “average” specimen is not appropriate. Additionally, variations in the maximum stretches used during testing lead to experimental data that are not uniform in either stretch or stress. To address this, we adopted a methodology previously outlined in [24]. Specifically, we first obtained the constitutive model parameters for each specimen by fitting Eqs. (10) and (11) to the stretch-controlled experimental data from all protocols. With the model parameters thus determined, we then calculated stretches corresponding to a standardized set of stresses ranging from 1 to 100 kPa, increasing in 1 kPa increments. This was conducted for both longitudinal and circumferential directions, maintaining the ratios as per Section 2.4. By averaging the computed stretches at each predefined stress level, we could accurately depict the stress-stretch response curves for the “average” specimen and identify the biomechanical behavior at the 25th and 75th percentile ranges.

2.6. Physiologic state assessment

Arterial morphometry measurements and constitutive parameters were used to evaluate the physiologic stress-stretch state of the arterial segments while accounting for the residual deformations and internal pressure. A detailed description of the associated kinematic framework can be found elsewhere [23,28]. Briefly, the deformation gradient for the transition from the stress-free state to the physiologic state at luminal pressures of 80, 100, and 120 mmHg is defined as $\mathbf{F}_{phys} = diag\left[\frac{\partial r}{\partial R}, \frac{r}{R}\mathrm{K}, \lambda_z^{pre}\right]$, where R and r denote the stress-free radially-cut ring and the radius of the pressurized artery, respectively. The parameter $\mathrm{K} = \frac{2\pi}{2\pi - \alpha}$ quantifies the cut ring’s opening angle α, while λ_z^{pre} is the physiologic longitudinal pre-stretch, which represents the ratio of the *in situ* artery length to the length of the foreshortened excised arterial segment [20]. To measure the *in situ* longitudinal pre-stretch for each of the seven analyzed arterial segments, it is necessary to transect and recover them individually. However, our objective was to image the entire artery integrally using μCT before sectioning, which precluded direct measurements of the *in situ* longitudinal pre-stretch. To circumvent this, we investigated the relationship between the *in situ* pre-stretch measured for the FPA and the axial stretch at 100 kPa in a larger set of 125 human FPAs that we published previously [21]. Our analysis revealed a robust linear relationship between pre-stretch (λ_z^{pre}) and axial stretch at 100 kPa (λ_z^{100kPa}), characterized by an R^2 of 0.53. Using this relationship ($\lambda_z^{pre} = 0.8347 \cdot \lambda_z^{100kPa} + 0.1801$), we estimated the *in situ* pre-stretch values for each of the seven analyzed arterial segments. Alternatively, the decoupling stretch method could have been employed to find the pre-stretch value at which the axial force becomes independent from the internal luminal pressure, typically using a nonlinear least-squares method. This value is often assumed to approximate the *in situ* longitudinal pre-stretch for the FPA and other larger vessels [23,32] when direct measurement is not feasible. However, this approach yielded unphysiologically high axial stress values in a significant portion of the smaller tibial artery specimens, and thus was deemed unsuitable for our analysis.

All physiologic parameters were determined assuming tissue incompressibility and no perivascular tethering, i.e., zero pressure on the outer surface of the artery, and by using the equilibrium equations from the balance of linear momentum. The calculated physiologic

parameters included the stored elastic energy associated with the deformation of the artery from diastole to systole (ΔW), and the circumferential stretch experienced by the vessel during the cardiac cycle ($\lambda_\theta^{cardiac}$), which was calculated by dividing the mid-line radius at 120 mmHg by the radius at 80 mmHg. Additionally, we calculated the physiologic circumferential stiffness (E_θ) as the change in the average circumferential physiologic stress between systole and diastole divided by the change in the average circumferential stretch:

$$E_\theta = \frac{t_{\theta\theta}^{phys,avg}(sys) - t_{\theta\theta}^{phys,avg}(dias)}{\lambda_\theta^{phys,avg}(sys) - \lambda_\theta^{phys,avg}(dias)}. \quad (16)$$

Here $t_{\theta\theta}^{phys,avg}$ and $\lambda_\theta^{phys,avg}$ represent the average through-thickness circumferential physiologic Cauchy stress and stretch, calculated by integrating them over the current volume and dividing by the total current volume [23,28].

2.7. Structural analysis

To account for directional differences in structure, we performed structural analysis using both transverse (circumferential) and ~ 1 cm-long longitudinal sections adjacent to the mechanically tested segments. All specimens were preserved in methacarn for a minimum of 48 h and subsequently transferred to 70 % ethanol for another 48 h. Following this, the arteries were embedded in paraffin, sectioned 5 μm thick, and stained with Movat Pentachrome to quantify elastic fibers (black color) and glycosaminoglycans (GAGs, greenish-grey color), and with Masson's Trichrome (MTC) stain to quantify collagen (blue color) and SMCs (red color). Slides were scanned at 10x resolution and analyzed using our custom-designed software that allows measurements of constituent fractions [28,33]. The tunica media's thickness was measured using transverse sections to account for regional variations along the vessel circumference. The thickness of the external elastic lamina (EEL) was evaluated using longitudinal sections because it contained predominantly longitudinally-oriented elastic fibers [21]. The fraction of these elastic fibers within the EEL was assessed using Movat Pentachrome stains. Our previous analysis indicated directional variations in medial GAGs [28], hence GAGs were measured using both transverse and longitudinal Movat Pentachrome sections. Collagen and SMCs in the tunica media were assessed using MTC stains and both transverse and longitudinal sections.

To put structural information in the context of vascular disease, we have also graded each of the seven arterial segments using a six-stage peripheral pathology scale described previously [20–22]. Briefly, stage I represented a healthy artery devoid of calcification or intimal thickening; stage II was associated with minor intimal thickening and SMCs proliferation, but without calcification or significant atherosclerotic plaques; vessels in stage III demonstrated pronounced intimal thickening with limited protrusion into the lumen, but lacked calcification; arteries of stage IV exhibited focal calcification, pools of extracellular lipid, or plaques with <30 % protrusion into the lumen; stage V included arteries with severe medial calcification, stenosis >75 %, and large lipid pools; stage VI represented end-stage disease with extreme calcification and luminal occlusions. A total of 104 specimens were

evaluated using this scale, and a single operator performed all the grading to minimize variability.

2.8. Statistical analysis

The statistical analysis was conducted to evaluate: 1) differences between the above-knee SFA and PA; 2) differences among below-knee AT, PT, and FA; 3) differences between the transition segments of the AT arch and TPT; 4) differences between above-knee arteries and transition zones; 5) differences between below-knee arteries and transition zones; and 6) differences between above and below-knee arteries. Initially, for the first objective, we assessed the normality of differences between the SFA and PA using the Shapiro-Wilk test. Subsequently, a paired *t*-test was performed for normally distributed data ($p \geq 0.05$), or a non-parametric Wilcoxon Signed-Rank test was utilized for non-normally distributed data ($p < 0.05$). To address the second objective, we evaluated the normality of differences between AT and PT, AT and FA, and PT and FA. If normality was confirmed, a one-way repeated measures ANOVA was executed. Significant differences identified by ANOVA led to post-hoc analysis using Tukey's Honestly Significant Difference to determine pairwise differences while controlling for Type I error across multiple comparisons. For non-normally distributed differences, we applied the non-parametric Friedman test as an alternative to the one-way repeated measures ANOVA. The assessment of differences between transition segments mirrored the approach taken for the SFA and PA. For objectives 4), 5), and 6), we calculated average values for each segment across all subjects - for instance, averaging SFA and PA values for above-knee assessments, and AT, PT, and FA for below-knee. These average values were then subject to normality assessment, followed by either a paired *t*-test or a Wilcoxon Signed-Rank test to determine the significance of the differences.

When appropriate, we have also performed multiple linear regression analysis, with subject demographics and risk factors serving as independent variables to predict the overall vascular pathology or the calcification specifically. Age, BMI, and the extent of calcification, quantified as the volume fraction within each arterial segment, were treated as continuous variables. Sex, HTN, DM, DLD, and CAD were considered nominal variables, whereas smoking status and the severity of vascular pathology were classified as ordinal variables. A stepwise linear regression approach was utilized to determine statistically significant predictors, allowing variables to enter the model when the significance level of their F-value was less than 0.05 and to be removed from the model when the significance exceeded 0.10. Results are presented as mean or median and standard deviation, where appropriate. All analysis was done in IBM SPSS Statistics v25 (IBM, Armonk, NY).

3. Results

3.1. Arterial specimens

Vascular pathology of the specimens is summarized in Table 1. The majority of the specimens were of stages II to IV, seven specimens were of stage I (completely healthy artery devoid of calcification or intimal thickening), and none were of stage V or VI (severe and widespread calcification, stenosis, or aneurysmal dilatation; entirely calcified vessel or complete occlusion). Diabetes (DM) and age accounted for 57 % of the variability in

SFA pathology, while dyslipidemia (DLD) explained 42 % of the variability in PA disease. Hypertension (HTN) accounted for 41 % of the variability in the pathology of the TPT. No statistically significant predictors were identified for the AT arch or the tibial vessels.

Fig. 2 demonstrates 3D μCT images of all analyzed arteries. The top row represents 8 non-calcified arteries, and the bottom row depicts 7 arteries in which calcification was detected. The percentage of calcification by volume in mechanically analyzed segments (marked with black boxes) is provided for each specimen, along-side its age and sex. Of all arterial segments, 40 % were devoid of calcification. In the remainder, the SFA contained 4 % to 7 % calcium by volume and the PA less than 1 %. Below the knee, the FA had up to 5 %, PT up to 2 %, and AT less than 1 %. The transition zones of the TPT and AT arch contained up to 4 % of calcification by volume. Among the seven arteries that presented with calcification, four exhibited calcification both above and below the knee, whereas the remaining three showed calcification exclusively below the knee. None of the arteries demonstrated calcification solely in the suprapopliteal region. DM and coronary artery disease (CAD) explained 78 % of the variability in calcification in the SFA, and CAD accounted for 39 % in the PA. Below the knee, DM and male sex explained 58 % of the variability in the FA calcification, while DLD and smoking explained 62 % in the AT arch. No statistically significant predictors were observed for the AT and PT.

Average values of the inner arterial diameter, load-free and stress-free wall thicknesses, and longitudinal and circumferential opening angles for different arterial segments are summarized in Table 2, along with their standard deviations. The diameter decreased along the length of the artery, changing from 5.60±2.41 mm in the SFA to 2.05±0.42 mm in the FA. The SFA had a 29 % larger diameter compared to the PA ($p = 0.001$). The AT artery's diameter was 15 % greater than that of the PT ($p = 0.047$) and 22 % larger compared to the FA ($p = 0.011$); however, the PT and FA diameters showed no significant difference ($p = 0.364$). In the transition zones, the TPT exhibited a 19 % larger diameter relative to the AT arch ($p = 0.032$). The diameters of the above-knee arteries exceeded those of the transition zones by 58 % ($p < 0.001$), whereas the below-knee arteries were 40 % smaller ($p < 0.001$). Collectively, the diameters of the above-knee arteries were more than twice that of the below-knee arteries ($p < 0.001$).

Regarding arterial wall thickness, no significant differences were observed between the SFA and PA in both load-free ($p = 0.171$) and stress-free ($p = 0.934$) states. The below-knee tibial arteries also showed similar thickness in the load-free state ($p = 0.063$), but in the stress-free state, the AT was 15 % thicker than the FA ($p = 0.043$). The wall thickness in the transition zones did not differ significantly in either state ($p = 0.414$ for load-free, $p = 0.642$ for stress-free); however, the above-knee arteries were thicker by 22 % and 19 % than the transition zones in the load-free ($p < 0.001$) and stress-free ($p < 0.001$) states, respectively. Comparatively, the below-knee tibial arteries were 14 % and 29 % thinner than the transition zones in load-free and stress-free states, respectively ($p < 0.001$ for both). Furthermore, the above-knee arteries had 53 % and 57 % greater thickness than the below-knee arteries in load-free ($p < 0.001$) and stress-free ($p < 0.001$) states, respectively.

No significant differences were noted in the circumferential or longitudinal opening angles among any of the vessel groups. Specifically, for the SFA and PA, the p-values were 0.945 and 0.404, respectively; for the below-knee tibial arteries, the p-values were 0.052 and 0.579; and for the transition zones, the p-values were 0.266 and 0.373 for circumferential and longitudinal opening angles, respectively. Additionally, opening angles of the above and below-knee arteries did not significantly differ from those of the transition zones ($p = 0.119$ and $p = 0.627$ for circumferential, $p = 0.388$ and $p = 0.108$ for longitudinal) or the below-knee tibial arteries ($p = 0.382$ and $p = 0.488$ for circumferential and longitudinal directions, respectively).

3.2. Biaxial mechanical properties

Equibiaxial stress-stretch curves for all the evaluated specimens, segmented by type, are summarized in Appendix Fig. 10, Fig. 11, and Fig. 12. Due to technical errors – namely, device malfunctions and specimen detachment - four of the 104 specimens were omitted from the analysis. Arteries with disease stage of III or higher are denoted by a circle with a horizontal line, while those containing calcium are marked with a vertical line; specimens displaying both characteristics are identified by a cross.

Arteries located below the knee were more frequently diseased or calcified than those situated above the knee. Specifically, only three segments each from the SFA and PA exhibited either atherosclerotic disease or calcification. In contrast, below the knee, five AT, four PT, and three FAs were either diseased or calcified. Notably, the highest incidence of pathology was observed in the AT arch transition zone, accounting for almost half (seven) of the total specimens.

In arteries located above the knee, both calcification and disease seemed to contribute to increased circumferential stiffness. This trend was also evident in the transition zones but not in the below-knee arteries. The constitutive model fits yielded an R^2 exceeding 0.91 for all specimens, and 95 % of the specimens demonstrated an R^2 greater than 0.95. The average R^2 was 0.986. Constitutive model parameters are summarized in Appendix Table 6, and these parameters were used to generate the stress-stretch curves representing the average specimens.

Stress-stretch curves representing the average specimens (solid curves) and samples in the 25th and 75th percentiles (shaded areas) are presented in Fig. 3. The data are presented for the above (SFA, PA) and below-knee (AT, PT, FA) arteries in panels A) and B), while the transition zones (Arch and TPT) are plotted separately in panels C) and D). The arterial segments were compared using stretches that correspond to equibiaxial Cauchy stresses at 25, 50, 75, and 100 kPa. Analysis revealed that the SFA exhibited ~20 % greater longitudinal stiffness compared to the PA, with statistical significance ranging from $p = 0.004$ to $p = 0.015$ across different stretch levels. In contrast, circumferential stiffness between the SFA and PA showed no significant difference ($p = 0.454$ to $p = 0.804$). The AT, PT, and FA demonstrated comparable stiffness, both longitudinally ($p = 0.074$) and circumferentially ($p = 0.152$ to $p = 0.375$). Within the transition zones, the AT arch was found to be ~35 % more compliant longitudinally compared to the TPT ($p = 0.033$ to $p = 0.041$), yet no significant difference was observed circumferentially ($p = 0.616$ to $p = 0.663$). Longitudinally, above-

knee arteries were 17–26 % less stiff than the transition zones ($p = 0.007$ to $p = 0.046$), with the disparity amplifying at higher stretches. Circumferentially, however, the stiffness of above-knee arteries did not significantly deviate from that of the transition zones ($p = 0.853$ to $p = 0.997$). The below-knee tibial arteries displayed markedly increased stiffness, being 83–96 % stiffer longitudinally than the transition zones ($p < 0.001$), and 29–49 % stiffer circumferentially ($p = 0.009$ to $p = 0.038$). Notably, the below-knee AT, PT, and FA were collectively more than twice stiffer than the above-knee SFA and PA longitudinally ($p < 0.001$ across all stretches). However, in terms of circumferential stiffness, the below-knee arteries were stiffer than the above-knee SFA and PA only at lower stretches corresponding to 25 kPa ($p = 0.018$) and 50 kPa ($p = 0.047$) stress levels. This trend did not hold at higher stress levels of 75 kPa ($p = 0.089$) and 100 kPa ($p = 0.136$), where no significant differences in circumferential stiffness between the above and below-knee arteries were observed.

The constitutive parameters for the four-fiber family model that represent average specimens are summarized in Table 3, while parameters representing specimens in the 25th and 75th percentiles are provided in Table 4 and Table 5.

3.3. Physiologic state assessment

At mean physiologic pressure of 100 mmHg, influenced by longitudinal pre-stretch and residual deformations as determined by the opening angles, the inner diameters of the SFA and PA exhibited no significant differences (5.50 mm vs 5.14 mm, $p = 0.529$). However, the SFA's outer diameter was 13 % larger than that of the PA ($p = 0.02$). Within the below-knee tibial arteries, the AT demonstrated a 65 % larger inner diameter (2.82 mm vs 1.71 mm, $p = 0.020$), while the PT exhibited a 14 % larger outer diameter (4.12 mm vs 3.63 mm, $p = 0.010$) compared to the FA. The inner and outer diameters of the transition zones were not statistically different ($p = 0.555$, $p = 0.086$); however, collectively, they were ~40 % smaller than those of the above-knee arteries ($p < 0.01$), and featured a 46 % larger lumen and a 29 % larger outer diameter than the below-knee arteries (both $p < 0.01$). Overall, the above-knee arteries had a 2.5-fold larger inner diameter (5.40 mm vs 2.15 mm) and 2.1-fold larger outer diameter (8.06 mm vs 3.84 mm) compared to the below-knee arteries (both $p < 0.01$).

Physiologic longitudinal and circumferential Cauchy stresses for each arterial segment at an internal pressure of 100 mmHg are presented in Fig. 4A,B. There were no significant differences in either longitudinal (t_{zz}, $p = 0.927$) or circumferential ($t_{\theta\theta}$, $p = 0.976$) stresses between the SFA (42 kPa longitudinal, 33 kPa circumferential) and PA. Similarly, stresses in the below-knee AT, PT, and FA did not significantly differ in longitudinal ($p = 0.732$) or circumferential ($p = 0.144$) directions. Longitudinally, stresses in the transition zones were comparable to those in the above-knee arteries ($p = 0.394$), but were 37 % lower compared to the below-knee arteries ($p = 0.009$, 39 kPa vs 62 kPa). Circumferentially, transition zone stresses showed no significant differences compared to stresses in either above (27 kPa vs 33 kPa $p = 0.091$) or below-knee arteries (27 kPa vs 24 kPa, $p = 0.583$). Collectively, the below-knee arteries exhibited 48 % higher longitudinal (62 kPa vs 42 kPa, $p = 0.021$) but 27 % lower circumferential (24 kPa vs 33 kPa, $p = 0.006$) stresses compared to the above-knee arteries.

Circumferential cardiac cycle stretch (Fig. 4C) – representing the arterial segment's deformation from diastole to systole – demonstrated no significant difference across any segments (SFA vs PA: $p = 0.454$, AT vs PT vs FA: $p = 0.506$, AT arch vs TPT: $p = 0.997$, above-knee arteries vs transition zones: $p = 0.508$). However, there was an observable trend towards a greater cardiac cycle stretch in the transition zones compared to the below-knee arteries ($p = 0.072$). Furthermore, above-knee arteries tended to experience marginally higher stretch than below-knee arteries overall (1.020 vs 1.014), nearing the threshold of statistical significance ($p = 0.051$).

The *in situ* longitudinal pre-stretch (Fig. 4D) was higher in the PA than in the SFA (1.311 vs 1.259, $p = 0.015$). However, no significant differences were observed among the below-knee tibial arteries ($p = 0.074$). Notably, the AT arch exhibited a 33 % higher pre-stretch than the TPT ($p = 0.040$). Additionally, the above-knee arteries demonstrated a 24 % higher pre-stretch compared to the transition zones ($p = 0.007$), which in turn had an 86 % higher pre-stretch than the below-knee arteries ($p < 0.001$). In aggregate, above-knee arteries exhibited longitudinal pre-stretch values that were 2.3 times higher (1.285 vs 1.123) than those of below-knee arteries ($p < 0.001$).

Variations in stored elastic energy throughout the cardiac cycle (Fig. 4E) exhibited to significant differences among any of the arterial segments (SFA vs PA: $p = 1.0$, AT vs PT vs FA: $p = 0.197$, AT arch vs TPT: $p = 0.744$, above-knee arteries vs transition zones: $p = 0.710$, below-knee arteries vs transition zones: $p = 0.232$). However, there was a noticeable trend of the above-knee arteries displaying greater changes in stored elastic energy during the cardiac cycle (0.715 kPa) compared to the below-knee arteries (0.449 kPa), although this trend did not achieve statistical significance ($p = 0.073$).

Finally, no statistically significant differences were observed in physiologic circumferential stiffness (Fig. 4F) - defined as the change in circumferential physiologic stress divided by the corresponding change in stretch during the cardiac cycle - between the SFA (766 kPa) and the PA (670 kPa) ($p = 0.133$). Similarly, the below-knee tibial arteries displayed no significant differences in stiffness ($p = 0.651$), and the stiffness levels in the transition zones were comparable ($p = 0.624$). However, the above-knee arteries were found to be 30 % stiffer physiologically than the transition zones ($p = 0.035$), though the latter exhibited stiffness levels similar to the below-knee arteries ($p = 0.123$). Overall, no significant differences were detected in physiologic circumferential stiffness between the above-knee and below-knee arteries ($p = 0.847$), with average values of 718 kPa and 754 kPa, respectively.

3.4. Structural analysis

Representative longitudinal and transverse histological sections of all evaluated segments above (Fig. 5) and below (Fig. 6) the knee, along with the transition zones (Fig. 7), obtained from the same 45-year-old male subject illustrate the differences in elastin (Movat), collagen (MTC), SMC (MTC), and GAGs (Movat) contents. Bidirectional histology illustrates the directionality of these components with longitudinal elastic fibers in the EEL and primarily circumferentially-oriented SMCs in all segments.

Results of the structural analysis for all above and below-knee segments are presented in Fig. 8. Panel A) demonstrates that the SFA exhibited a 7 % higher elastin density in the EEL compared to the PA (18% vs. 11 %, $p = 0.001$). However, no significant differences in elastin density were observed among the below-knee AT, PT, and FA ($p = 0.675$). Similarly, elastin content between the AT arch and the TPT was comparable ($p = 0.190$). There were also no significant differences in elastin content between the above-knee arteries and the transition zones ($p = 0.317$). Nonetheless, both the above-knee arteries and transition zones demonstrated significantly greater elastin density in the EEL than the below-knee arteries, with mean values of 15 % and 12 % versus 6 %, respectively ($p < 0.001$ for above-knee arteries vs below-knee arteries, and $p = 0.006$ for transition zones vs below-knee arteries).

No significant differences were observed in the thicknesses of the EEL (Fig. 8B) when comparing above-knee SFA and PA ($p = 0.570$) or among below-knee arteries ($p = 0.218$). Similarly, the transition zones of the AT arch and the TPT exhibited no significant variance in EEL thickness ($p = 0.161$). However, there was a notable decrease in EEL thickness from the above-knee region, averaging 134 μm, to the transition zones, averaging 98 μm ($p = 0.003$), and further to 80 μm in the below-knee region ($p = 0.001$). Despite this trend, the difference in EEL thickness between the below-knee arteries and the transition zones was not statistically significant ($p = 0.110$).

Longitudinal (Fig. 8C) and transverse (Fig. 8D) images revealed no significant differences in collagen content between the above-knee SFA and PA ($p = 0.148$, $p = 0.589$), within the transition zones ($p = 0.536$, $p = 0.329$), or among the below-knee AT, PT, and FA ($p = 0.239$, $p = 0.764$). The above-knee arteries had larger collagen content compared to the transition zones (36/34 % vs. 27/24 %, $p = 0.013/p = 0.002$). However, collagen levels in the below-knee arteries did not significantly differ from those in the AT arch and the TPT ($p = 0.399$, $p = 0.508$). Overall, the above-knee arteries had a collagen content that was ~10 % lower than that of the below-knee arteries ($p = 0.001$ for both longitudinal and transverse sections). Collagen content was consistent between longitudinal and transverse sections ($p = 0.329$).

The SMC content remained consistent along the arterial length, showing no significant changes in either longitudinal (all $p > 0.370$, Fig. 8E) or transverse (all $p > 0.148$, Fig. 8F) sections. However, transverse sections exhibited a higher overall SMC content (11 %) compared to longitudinal sections (7 %) ($p < 0.001$). Additionally, there were no significant differences in SMC content among the arteries above the knee ($p = 0.591$ for longitudinal, $p = 0.824$ for transverse), in the transition zones ($p = 0.796$ for longitudinal, $p = 0.932$ for transverse), or among the below-knee regions ($p = 0.431$ for longitudinal, $p = 0.807$ for transverse).

In transverse sections (Fig. 8G), GAG content did not vary significantly along the artery length ($p = 0.496$), nor did it differ significantly between the above-knee arteries ($p = 0.154$), transition zones ($p = 0.781$), or below-knee arteries ($p = p = 0.692$). However, the above-knee arteries exhibited a higher percentrage of GAGs (38 %) compared to both the transition zones (30 %, $p < 0.001$) and the below-knee arteries (31 %, $p = 0.003$) when assessed using transverse sections (Fig. 8H). Despite this, no significant differences were observed between

the SFA and PA ($p = 0.830$), within the transition zones ($p = 0.357$), or among the AT, PT, and FA ($p = 0.438$) when using these transverse sections. Notably, longitudinal sections displayed an overall higher GAG presence (39 %) compared to transverse sections (34 %) ($p < 0.001$).

In summary, the more proximal above-knee arteries exhibited significantly higher elastin ($p < 0.001$), thicker EEL ($p = 0.001$), increased collagen ($p < 0.001$), and more GAGs ($p = 0.003$) compared to the more distal below-knee arteries. However, there were no differences in the SMC content between these regions. The above-knee SFA had more elastin than the PA ($p = 0.001$) but was not different from it in any other structural characteristics. Among the below-knee AT, PT, and FA, no differences were observed in any structural characteristics. The transition zones demonstrated elastin content similar to the above-knee arteries, but the EEL thickness, collagen, SMC, and GAG content were more akin to those found in the below-knee arteries.

4. Discussion

As the global population ages, the prevalence of PAD continues to rise [34]. In the lower extremities, PAD predominantly manifests as occlusive disease, affecting arteries both above and below the knee. Suprapopliteal PAD, involving the SFA and PA, commonly presents with intermittent claudication and rest pain. It is more amenable to treatments like angioplasty and stenting, although they continue to leave significant room for improvement [6–12]. Conversely, infrapopliteal PAD affecting the tibial arteries frequently leads to critical limb ischemia, which is characterized by tissue loss and non-healing ulcers. Such cases often require aggressive interventions like bypass grafting and have a higher incidence of amputations compared to suprapopliteal PAD [7,13–17]. Recent evidence [35] suggests that the nature of obstructions in the arteries below the knee tends to be thrombotic or thromboembolic, with over half of stenosed IPAs showing limited atherosclerosis. This is contrary to the FPA constrictions that primarily have atherosclerotic origin [3]. The specific factors contributing to these variations between the FPA and the IPA diseases remain unclear, but a deeper understanding of the structural and mechanical differences in arteries above and below the knee could elucidate the disparate pathophysiology and aid in the development of more targeted therapies.

Our data demonstrate that IPAs were more frequently diseased or calcified compared to the FPA vessels from the same subjects. Among the factors contributing to suprapopliteal artery pathology, DM, age, and DLD were the major contributors, while HTN also influenced infrapopliteal artery disease. Notably, fewer than half of our middle-aged specimens were devoid of any arterial calcification, with DM and CAD being the primary contributors, further exacerbated by male sex, DLD, and smoking in specific segments. Epidemiologic studies have established DM, smoking, DLD, and HTN as the leading risk factors of PAD [36,37], though differentiation between risk factors specific to the FPA and IPA is rarely investigated.

The influence of DM on PAD is multifactorial [38]. It involves a range of contributing factors, including glycation of proteins and lipids, which alters their normal functions and

leads to increased arterial stiffness [27]. Insulin resistance impairs endothelial function, while disruptions in lipid metabolism and chronic inflammation add to the disease complexity. Other contributing factors include hypercoagulability, endothelial and SMC dysfunction, microvascular disease, and neuropathy. These mechanisms increase the risk of ulceration and contribute to a generalized dysfunction of the autonomic nervous system of PAD patients with DM. Notably, DM has a particular impact on smaller vessels, such as those located below the knee, as well as the microvasculature.

Cigarette smoking similarly impacts PAD through endothelial cell dysfunction, oxidative stress, inflammation, platelet aggregation, reduced oxygen delivery, vasoconstriction, SMC remodeling and macrophage phenotypic transformation [39,40]. The effects of DLD on PAD development have also been described, although the lipid risk profiles of PAD and CAD have some key differences [41]. Measures like elevated total cholesterol and decreased high-density lipoprotein cholesterol are strongly associated with PAD, but the correlation between low-density lipoprotein cholesterol and PAD is less straightforward [41]. Interestingly, plaque composition in the lower extremity arteries is distinct from that in CAD, exhibiting more fibrous components and less lipid content [42]. Lastly, the impact of HTN on PAD is commonly thought to involve similar mechanisms of endothelial dysfunction, inflammation, and increased vascular stiffness. However, conflicting evidence exists regarding optimal blood pressure goals in PAD patients [43,44], as some studies suggest adverse outcomes with low blood pressure, and no specific antihypertensive drug class has demonstrated clear benefits in the PAD population.

One of the potential reasons for the limited effectiveness of drug therapies could be related to the prevalence of vascular calcification – one of the characteristic features of lower extremity artery PAD. Vascular calcification of the FPA has a profound effect on circumferential stiffness, rendering many vessels with advanced mineralization non-compliant. We have previously described these effects in the above-knee FPA [22] and have observed similar findings in our current SFA and PA specimens. Calcification in the arteries of the lower extremity often manifests as concentric rings that fuse over time into larger sheets and plates [3]. This dramatically increases stiffness [22,27], rendering 40-year-old diabetic FPA as stiff as arteries from individuals older than 70 years without DM [27]. A potential mechanism for this is the osteoblastic transformation of primarily circumferentially oriented SMCs under the hyperglycemic conditions characteristic of DM that results in the formation of ring-like calcium deposits [45]. As these calcium deposits coalesce over time, the longitudinal stiffness of the vessel increases as well – an effect further amplified by DM-induced glycation of elastic fibers [46] and collagen cross-linking. Surprisingly, we have not observed these effects in the IPA vessels evaluated in the present study, possibly due to their already higher stiffness compared with the FPA. Importantly, lower extremity artery calcification poses significant challenges to drug delivery [47] and angioplasty, likely contributing to the quadrupled risk of amputation observed in calcified lower extremity arteries [48], and it is particularly prevalent below the knee.

Among the below-knee arteries, the AT and the PT were more frequently affected by disease compared to the FA. This observation aligns with previous studies, which also reported a higher prevalence of pathology in the AT and PT relative to the FA [49–51].

Interestingly, ethnicity has been reported to influence this pattern [52]. The PT supplies various muscles and tissues, including those in the sole of the foot, while the AT serves the anterior compartment of the leg and the dorsal part of the foot. Both typically have more branches and higher resistance than the FA, which supplies the lateral compartment of the leg. Consequently, they experience greater metabolic demands and increased susceptibility to ischemic conditions that favor the development of pathology. Interestingly, an even higher incidence of pathology was observed in the transition zone of the AT arch, which was affected in nearly half of our middle-aged specimens. Anatomically, the AT is distinct from other tibial vessels. After branching off from the PA, it traverses the superior aspect of the interosseus membrane. This segment likely undergoes significant deformations during limb flexion, but little research has been conducted to characterize these deformations in the below-knee arteries, in contrast to the many studies of the FPA [53,54,54–56].

In addition to biomechanical distinctions, IPA vessels exhibit smaller diameters and thinner walls than the FPAs. In the specimens examined in our study, the unloaded diameter decreased from 5.6 mm in the SFA to 2.1 mm in the FA, while the wall thickness similarly declined from 1.8 to 1.1 mm. At a physiologic pressure of 100 mmHg, midline diameter values changed from 7.3 mm in the SFA to 6.5 mm in the PA, 3.3 mm in the AT and PT, and 2.7 mm in the FA. These measurements are in good agreement with the MR-measured values from a large cohort of subjects with similar ages [50]. The smaller diameter of IPA vessels, when compared with the FPA, may contribute to increased vascular pathology through various mechanisms. These include a higher resistance to blood flow, which may induce greater stress on the endothelium, as well as altered blood flow profiles [57–59]. The IPA's smaller diameter also renders it more susceptible to inflammatory processes [60]. In larger vessels like the FPA, blood flows in laminar layers, with the blood near the center of the vessel moving quicker than the blood that is in contact with the arterial wall [58]. This flow pattern minimizes the interaction time between circulating inflammatory markers and the endothelial surface [61]. Conversely, in smaller IPAs, the reduced arterial diameter permits blood components, including inflammatory markers, to maintain more frequent and prolonged contact with the endothelial lining [59]. This increased contact time could potentially contribute to a higher inflammation risk and result in a greater predisposition for vascular pathology [60–63].

We have also observed significant differences in the mechanical properties of suprapopliteal and infrapopliteal arteries within the same subjects. Specifically, the SFA and PA were less stiff longitudinally than circumferentially - a trend we have reported previously in specimens across various age groups [23,24,27]. In contrast, the AT, PT, and FA were notably stiffer longitudinally but had similar circumferential compliance to the SFA and PA. The higher longitudinal stiffness in the arteries below the knee resulted in their more isotropic response under equibiaxial loads. Interestingly, the transition zones between the FPA and IPAs displayed considerable variability in mechanical characteristics, especially in the longitudinal direction. This variability suggests that the transition from the PA to the infrapopliteal vessels could differ among individuals. Existing literature provides scant information on the biaxial mechanical characteristics of human IPAs. Our own study [64], which focused on severely diseased human tibial arteries from patients with critical limb ischemia, reported significant nonlinearity and anisotropy. These tibial arteries were stiffer

circumferentially than longitudinally and exhibited decreased longitudinal compliance with increasing distal location. While our prior work included only three IPA specimens, the findings are consistent with the data presented here, as IPAs also exhibited less than 1.2 stretch at 100 kPa equibiaxial stress.

Differences in both morphology and intrinsic mechanical properties have led to distinct physiologic characteristics between the suprapopliteal and infrapopliteal vessels. Specifically, the arteries below the knee experienced physiologic longitudinal stresses that were 48 % higher than those above the knee, but 27 % lower circumferential stresses. There were no statistically significant differences in the cardiac cycle stretch, physiologic circumferential stiffness, or changes in stored elastic energy over the cardiac cycle between these regions. Previous research [21,23] indicates that middle-aged FPAs typically undergo 60–75 kPa of longitudinal stress and 35–40 kPa of circumferential stress. Our current findings reveal somewhat lower values - 42 kPa for longitudinal and 33 kPa for circumferential stress - likely attributable to subject-specific variations. Nevertheless, tibial arteries from the same subjects exhibited 62 kPa and 24 kPa longitudinal and circumferential stresses, respectively. Interestingly, despite their higher longitudinal stress, the IPAs exhibited smaller longitudinal pre-stretch values than the SFA or the PA, registering at an average of 1.123 compared to the average of 1.285 for the FPA. These pre-stretch values for the SFA and PA align well with data previously reported for a similar age group [20,23]. Additionally, the small values of cardiac cycle stretch, which remained below 1.02 for most arterial segments, also align closely with earlier findings for a similar demographic [21,28].

These physiologic findings are particularly interesting in the context of structural disparities between the FPA and IPAs. Specifically, our data demonstrate that the more proximal SFA has a greater elastin content in the EEL compared to the more distal PA. This, however, was the sole structural difference observed between these suprapopliteal vessels. Recent studies [21] corroborate these findings, indicating no significant structural or mechanical differences between the distal PA and the more proximal SFA when both segments are either healthy or similarly affected by disease. Information on the structural characteristics of healthier middle-aged IPAs remains scarce, as amputation specimens from subjects with critical limb ischemia present challenges for structural assessments, as the pathology often obscures the inherent characteristics of the arteries [3,65]. Our findings, derived from both healthy and mildly diseased IPAs, show that these arteries are structurally distinct from the FPAs but remarkably similar to each other.

For instance, IPAs have less elastin content and a thinner EEL compared to their FPA counterparts. Prior research has shown that FPAs experience significant deformations during limb flexion, necessitating specialized structural and mechanical features that accommodate a range of movements, such as axial compression, bending, and torsion [53,54,54–56]. One such specialized feature is the presence of longitudinally-oriented elastic fibers in the EEL, which enable the artery to handle the deformations induced by limb flexion [20,54]. Our previous research [21] indicated that the EEL of the FPA comprises approximately 40±20 % elastin at 13 years of age, decreasing to about 20±10 % by the age of 90. The current study’s measurements in middle-aged FPAs - averaging 18 % for the SFA with a range of

8–33 %, and 11 % for the PA within a 4–17 % range - align with these earlier findings while presenting slightly lower percentages. These results are to be expected due to the variations in demographics of the subject populations and the inherent subjectivity involved in histological quantification techniques. The IPAs seem to demonstrate reduced mobility during limb flexion, although additional research is needed to evaluate this speculation, with the notable exception of the AT arch that spans the interosseous membrane. Our structural analysis demonstrates that to facilitate these deformations, the AT arch contains 2.4-fold more longitudinally-oriented elastin than the AT and 2.1-fold more than the PT. It also exhibits a 33 % larger longitudinal pre-stretch compared to the TPT, presumably to accommodate enhanced axial deformations during limb flexion. Elastin is a mechanically and chemically stable protein with a long half-life of 74 years [66]. It is believed to be formed primarily during mid-to-late gestation and early postnatal periods [67–73]. As the tissue grows to maturity, elastic structures accumulate significant tension [20], which allows the artery to accommodate axial compression during locomotion, and enables greater intrinsic longitudinal compliance in the FPA compared to the circumferential direction. It also offers context for our findings of greater longitudinal stiffness in IPAs that have less longitudinal elastin than the FPA.

Furthermore, we found that IPAs had approximately 34 % less medial collagen than FPAs, while the SMC content remained consistent across all arterial segments. As anticipated, the SMCs in IPAs are oriented primarily circumferentially, similar to their orientation in the FPAs [28,74]. Lastly, we observed a higher GAG content in the arteries above the knee, as well as a directional dependence with greater content in the transverse sections. A similar trend has been reported previously for the FPA [28]. While the exact functions of these long unbranched polysaccharides in arterial tissues are not fully understood, they are often found attached to proteins, forming proteoglycans, and are thought to contribute to a range of functions, including water retention, regulation of cell behavior such as adhesion, proliferation, and migration, filtration, signal transduction, inflammation, fiber recruitment and arterial wall mechanics [75–77].

No study is complete without acknowledging its limitations, and our study is no exception. First and foremost, we used a purely elastic approach to analyze our specimens, neglecting their viscoelastic characteristics. While viscoelasticity does impact the behavior of muscular arteries, the existing data on the viscoelastic behavior of the FPAs are scarce [78], constraining our ability to compare our findings with prior research. Although we made efforts to obtain a sufficiently large sample size for meaningful statistical analysis, the study's scope was limited by the logistical challenges of procuring and evaluating small tibial arteries compared to the more easily accessible SFA and PA. Consequently, we were able to test over 100 specimens, but these specimens were obtained from just 15 human subjects. This limited sample size poses a risk for overfitting and constrains our ability to examine the influence of factors such as sex and race on the results, despite their recognized status as risk factors for PAD [79,80,80]. However, we did attempt to control for age by focusing on primarily middle-aged donors without severe pathologies. Another limitation stems from the heterogeneous nature of vascular diseases in arteries. While we used μCT imaging to capture variations in disease states, these could still contribute to the observed variability in mechanical and structural characteristics, particularly in transition

zones. Finally, our analysis exclusively considered the passive mechanical properties of the vessels, overlooking the role of active SMC tone - a factor known to significantly influence arterial mechanics [81]. Measurements of the active SMC tone would require assessments of SMC viability, and necessitate the use of tissues obtained from live donors, which is much more logistically challenging. Despite these limitations, our study contributes valuable insights into the mechanical, structural, and physiologic variations between above-knee and below-knee arteries using specimens from the same individuals.

5. Conclusions

Above-knee and below-knee arteries exhibit distinct differences in size, structure, and mechanical properties, which consequently lead to variations in their physiologic behavior. Specifically, infrapopliteal arteries such as the AT, PT, and FA are generally smaller, thinner, and more prone to disease compared to the SFA and PA. These arteries also demonstrate increased longitudinal stiffness, potentially attributable to reduced elastin content, although their circumferential mechanical properties largely align with those of the FPA. Arteries located below the knee are subjected to greater longitudinal stresses, but lower circumferential stresses and longitudinal pre-stretch. They also exhibit similar cardiac cycle stretch and comparable variations in stored elastic energy throughout the cardiac cycle. Structurally, these arteries contain less collagen and GAGs, yet maintain similar SMC content compared to suprapopliteal vessels. Collectively, these data contribute to a better understanding of human lower extremity artery biomechanics and may serve as valuable groundwork for the development of more effective, region-specific medical devices for the treatment of PAD.

Acknowledgments

This work was supported in part by the NIH awards HL125736, HL147128, AG062198, and P20GM152301. The authors would also like to acknowledge Live On Nebraska for their help and support, and thank tissue donors and their families for making this study possible.

Appendix

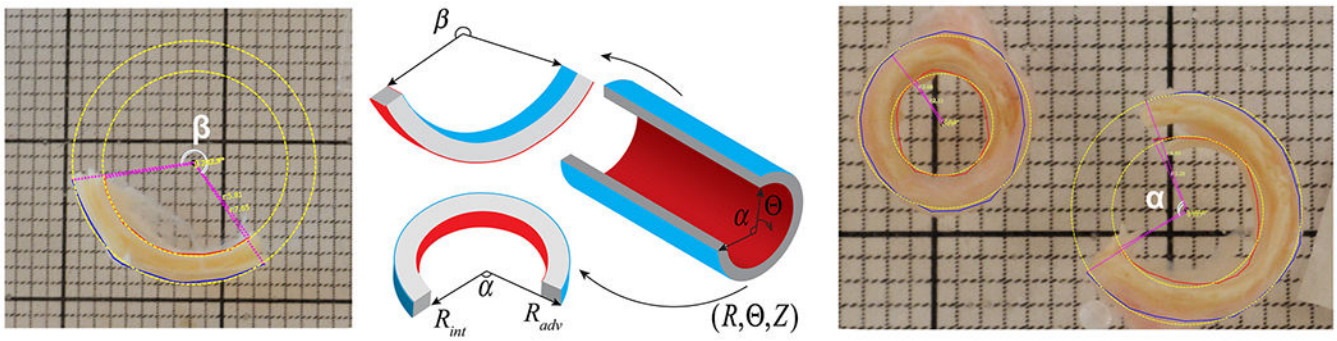

Fig. 9.

Morphometric measurements of the opening angle were conducted using custom-written software, which employs a least squares algorithm to fit a circle to the segmented outer and inner edges of the cut ring and axial strip of the arterial section. The circle's center is then

utilized to quantify the angle between the two edges of the sector. In this figure, yellow dashed lines indicate the best-fit circle, pink dots signify the circle's radius, and white curves depict the opening angle (α – circumferential, β – longitudinal). (For interpretation of the references to color in this figure legend, the reader is referred to the web version of this article.)

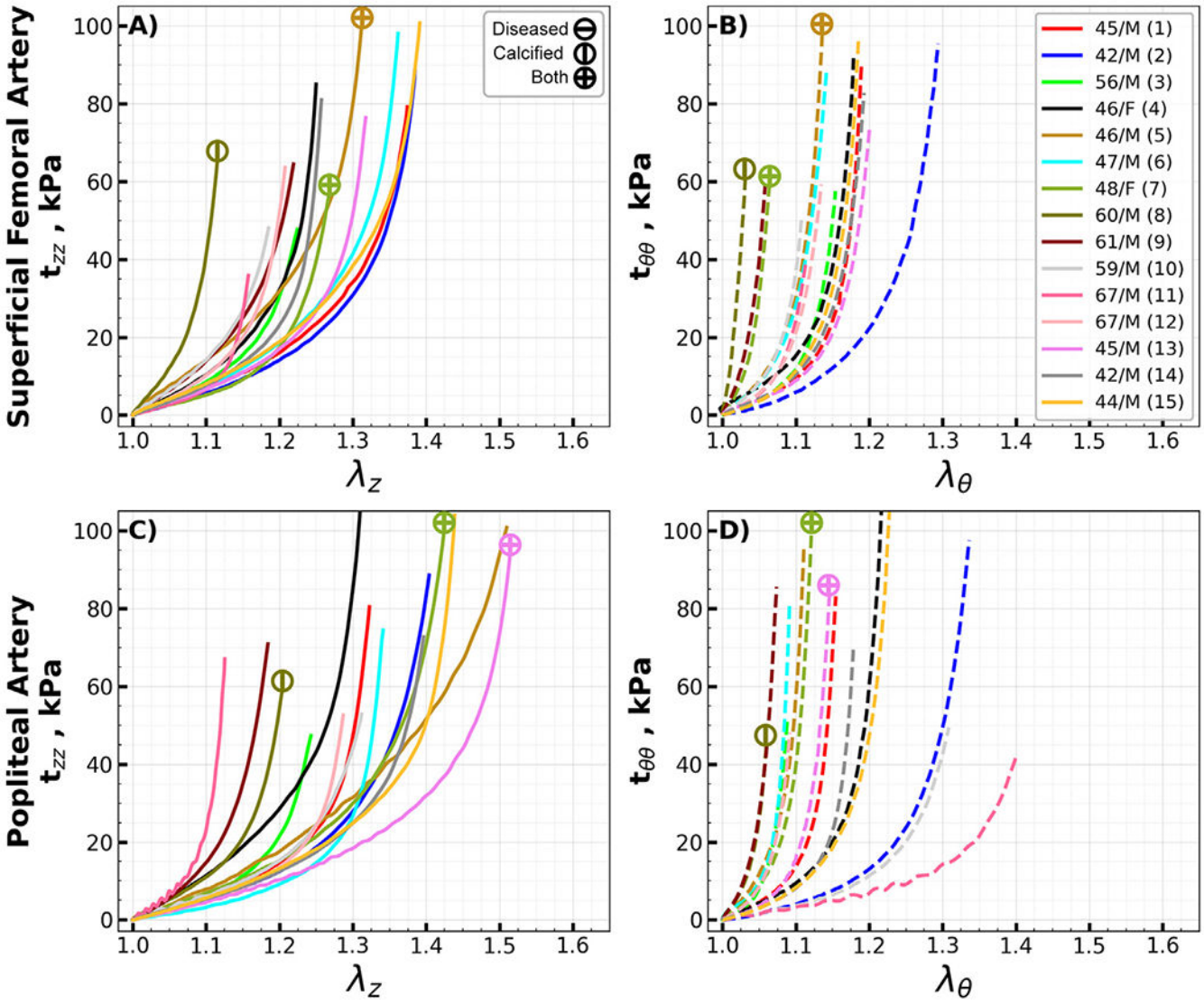

Fig. 10.

Equibiaxial Cauchy stress-stretch curves for all evaluated superficial femoral (SFA, A, B) and popliteal (PA, C, D) arteries in the longitudinal (z) and circumferential (θ) directions. Different colors represent different subjects. Arteries with atherosclerotic disease (disease stage greater than III) and calcified arteries (calcium volume greater than zero) are marked with circles containing horizontal and vertical lines, while circles with a cross represent arteries with both atherosclerosis and calcification. The age and sex of each subject are provided in the legend. (For interpretation of the references to color in this figure legend, the reader is referred to the web version of this article.)

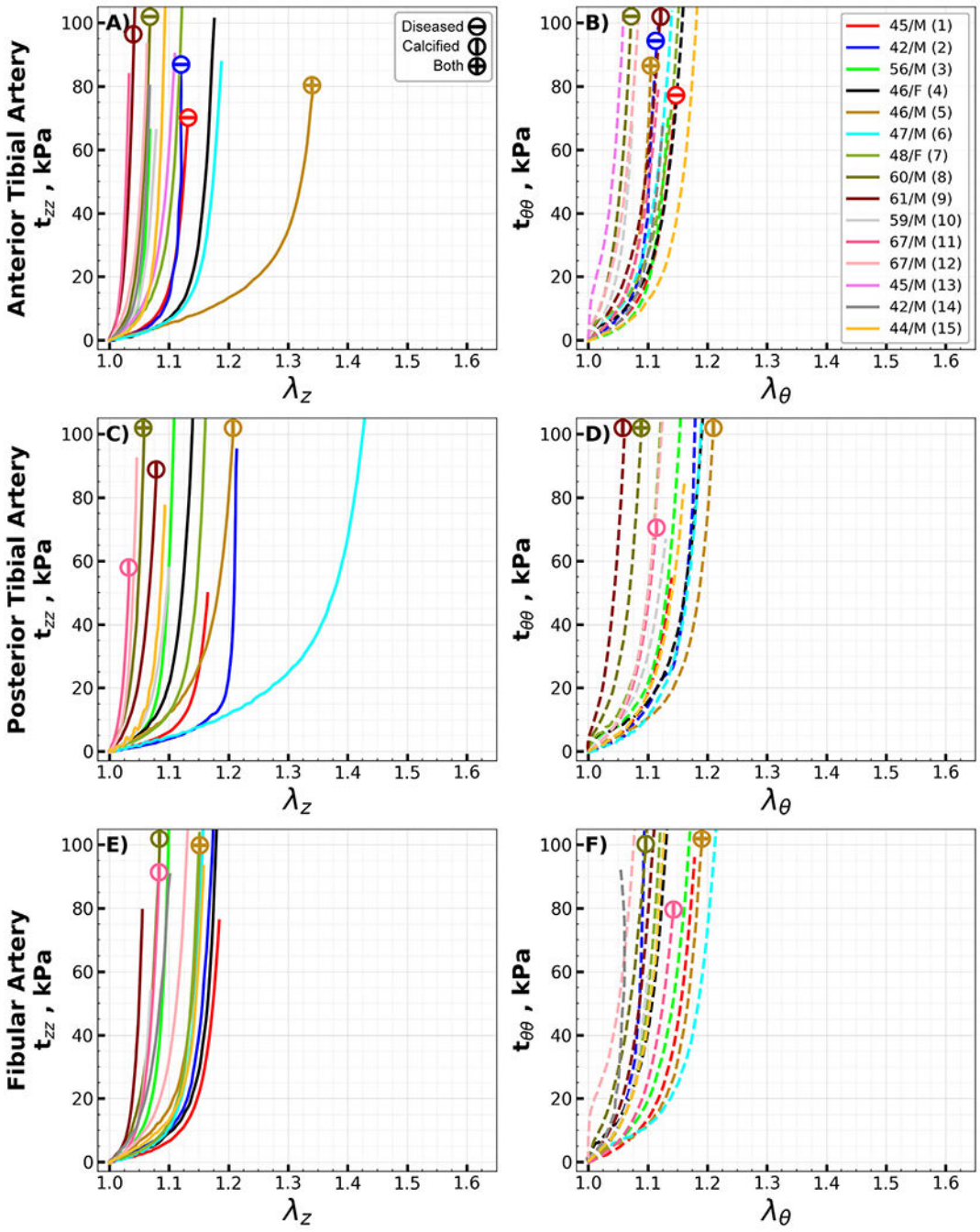

Fig. 11.

Equibiaxial Cauchy stress-stretch curves for all evaluated anterior tibial (AT, A, B), posterior tibial (PT, C, D), and fibular (FA, E, F) arteries in the longitudinal (z) and circumferential (θ) directions. Different colors represent different subjects. Arteries with atherosclerotic disease (disease stage greater than III) and calcified arteries (calcium volume greater than zero) are marked with circles containing horizontal and vertical lines, while circles with a cross represent arteries with both atherosclerosis and calcification. The age and sex of each

subject are provided in the legend. (For interpretation of the references to color in this figure legend, the reader is referred to the web version of this article.)

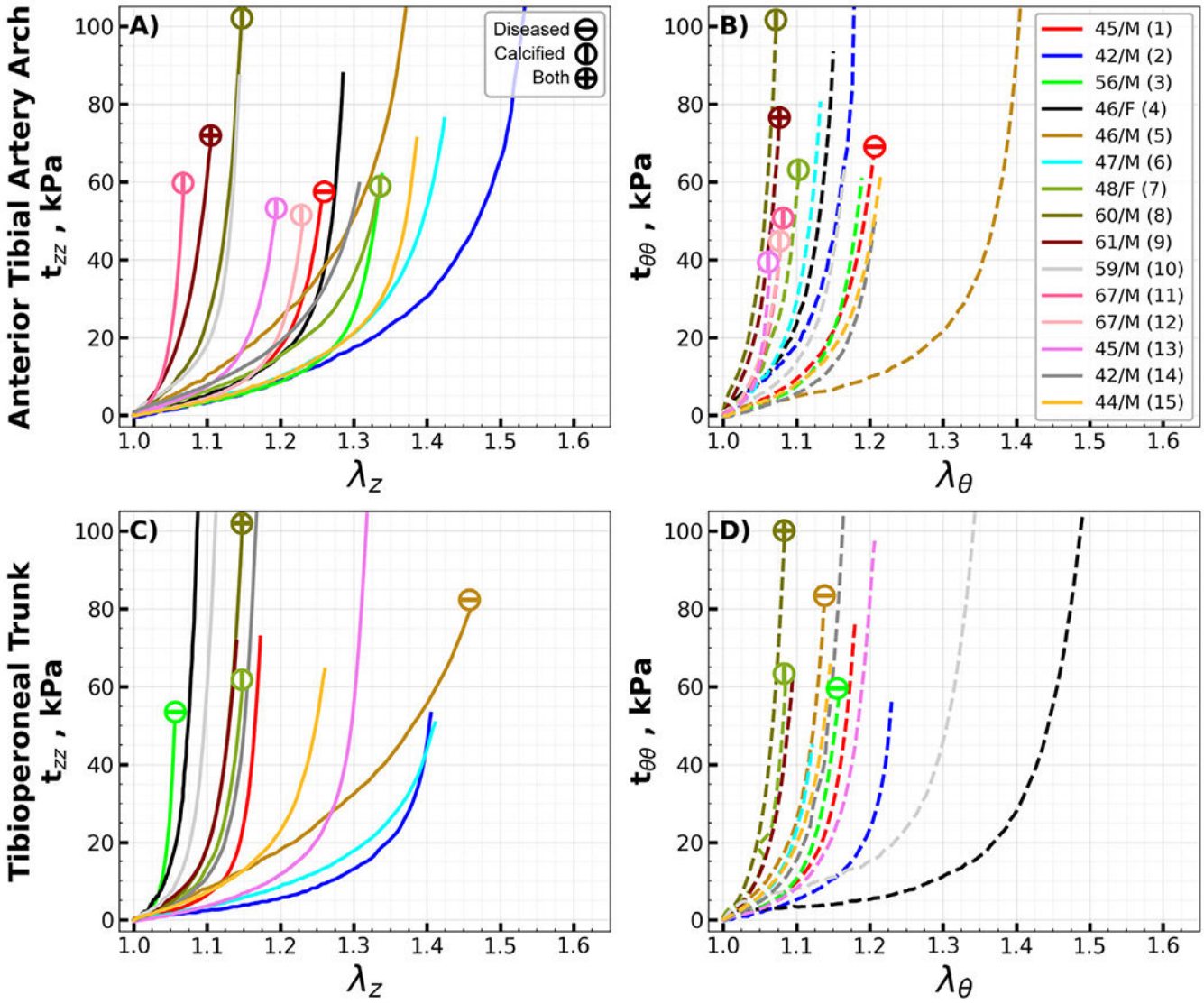

Fig. 12.

Equibiaxial Cauchy stress-stretch curves for the evaluated transition segments of the anterior tibial arch (A, B) and the tibioperoneal trunk (C, D) in the longitudinal (z) and circumferential (θ) directions. Different colors represent different subjects. Arteries with atherosclerotic disease (disease stage greater than III) and calcified arteries (calcium volume greater than zero) are marked with circles containing horizontal and vertical lines, while circles with a cross represent arteries with both atherosclerosis and calcification. The age and sex of each subject are provided in the legend. (For interpretation of the references to color in this figure legend, the reader is referred to the web version of this article.)

Table 6

Constitutive parameters for the four-fiber-family model for each specimen.

Location	No	Age, years	Sex	C_{gr}, kPa	C_1^{el}, kPa	C_2^{el}	C_1^{smc}, kPa	$C2smc$	C_1^{col}, kPa	C_2^{col}	γ, deg	R^2
SFA	1	45	M	9.88	8.07	1.28	4.94	15.52	1.82	9.34	55.76	0.989
	2	42	M	2.77	11.22	0.48	12.08	2.91	3.58	3.23	44.03	0.989
	3	56	M	7.75	14.41	1.38	9.37	19.88	1.59	15.99	39.54	0.989
	4	46	F	16.42	9.30	3.23	7.04	16.52	1.51	12.72	42.41	0.984
	5	46	M	20.91	15.10	1.47	18.66	25.48	0.85	17.67	49.73	0.986
	6	47	M	11.41	7.38	2.18	19.08	20.39	5.51	12.83	63.53	0.993
	7	48	F	7.44	4.61	3.63	54.68	59.94	9.26	29.83	55.75	0.983
	8	60	M	36.86	4.64	36.65	81.81	17.81	66.85	77.57	51.31	0.977
	9	61	M	17.03	17.26	4.31	69.25	64.41	19.57	35.85	61.32	0.997
	10	59	M	12.51	23.84	4.33	21.19	23.13	4.42	31.54	58.87	0.996
	11	67	M	7.78	1.85	21.29	17.24	23.28	2.44	36.10	44.81	0.997
	12	67	M	8.89	14.46	6.51	22.11	18.47	1.27	27.59	50.88	0.996
	13	45	M	5.96	10.55	1.23	9.72	9.98	3.45	6.64	43.06	0.986
	14	42	M	9.72	3.79	7.22	6.93	13.40	3.89	9.21	53.15	0.986
	15	44	M	7.84	14.68	0.74	9.96	10.95	2.26	10.93	61.28	0.993
PA	1	45	M	8.49	6.52	1.81	10.16	20.01	1.08	14.92	49.32	0.992
	2	42	M	4.59	7.82	0.88	4.39	2.80	2.14	3.74	49.87	0.996
	3	56	M	5.22	9.91	3.49	24.56	46.53	3.88	26.92	52.07	0.993
	4	46	F	12.78	15.75	1.84	5.45	10.16	0.89	12.72	54.23	0.996
	5	46	M	11.85	12.13	0.29	38.85	21.34	2.44	19.36	64.84	0.995
	6	47	M	5.56	1.00	4.56	30.03	21.93	5.76	23.67	59.41	0.982
	7	48	F	10.90	6.54	1.16	22.29	16.36	5.12	16.35	62.00	0.991
	8	60	M	12.95	12.10	6.74	46.60	70.92	7.48	41.24	54.71	0.996
	9	61	M	8.19	24.14	5.35	66.00	56.22	20.16	31.43	54.77	0.994
	10	59	M	3.83	11.23	1.32	3.69	3.12	2.55	3.36	49.50	0.990
	11	67	M	3.98	21.99	18.05	3.45	1.04	2.59	17.19	27.68	0.992
	12	67	M	7.98	2.94	5.33	14.05	55.30	4.74	26.08	63.09	0.991
	13	45	M	3.40	9.78	0.28	16.23	15.47	2.02	10.67	60.21	0.989
	14	42	M	6.87	6.90	0.93	4.84	11.77	2.15	9.94	57.79	0.988
	15	44	M	6.03	8.31	0.59	7.82	7.71	2.61	5.14	53.68	0.982
Arch	1	45	M	3.91	4.53	6.05	14.13	7.86	4.11	6.61	44.02	0.996
	2	42	M	8.37	1.31	1.36	20.72	4.07	6.52	6.88	63.14	0.976
	3	56	M	4.53	2.76	3.14	10.09	10.46	1.31	9.71	52.11	0.992
	4	46	F	11.83	0.54	10.19	24.34	11.97	5.23	14.08	58.04	0.989
	5	46	M	7.71	17.22	0.74	1.77	2.45	1.98	3.17	47.63	0.980
	6	47	M	4.89	5.41	1.01	26.93	13.95	6.10	9.72	59.80	0.996
	7	48	F	8.68	7.44	2.06	39.12	17.63	8.82	20.50	67.68	0.994
	8	60	M	17.61	10.62	24.92	97.74	42.19	34.89	35.74	53.41	0.989

Location	No	Age, years	Sex	C_{gr}, kPa	C_1^{el}, kPa	C_2^{el}	C_1^{smc}, kPa	$C2smc$	C_1^{col}, kPa	C_2^{col}	γ, deg	R^2
	9	61	M	20.63	34.55	26.23	81.05	43.61	26.07	43.69	45.59	0.994
	10	59	M	15.64	11.82	27.02	10.37	11.94	1.74	30.12	51.33	0.989
	11	67	M	0.55	16.56	74.94	33.48	41.88	44.45	67.48	40.38	0.993
	12	67	M	3.79	2.08	10.32	27.02	14.22	18.22	21.44	56.56	0.990
	13	45	M	2.12	17.30	2.21	32.08	74.60	5.18	39.48	47.43	0.987
	14	42	M	5.60	15.93	0.79	2.74	10.73	2.59	7.86	52.18	0.996
	15	44	M	5.79	3.26	1.85	7.77	6.92	1.96	6.20	50.58	0.994
TPT	1	45	M	5.29	1.83	20.60	11.31	12.38	3.08	21.96	37.45	0.995
	2	42	M	4.43	1.38	2.32	6.40	5.59	0.62	7.83	55.41	0.991
	3	56	M	0.92	31.20	89.96	18.06	13.52	8.63	78.79	35.60	0.993
	4	46	F	0.81	24.88	45.77	4.26	1.40	42.76	28.48	12.96	0.936
	5	46	M	10.99	12.59	0.30	10.13	23.29	8.64	10.10	66.92	0.997
	6	47	M	1.48	8.24	0.93	16.67	23.86	11.26	6.52	66.64	0.977
	7	48	F	9.94	5.24	22.89	42.92	29.79	10.82	41.43	47.91	0.995
	8	60	M	1.38	23.97	15.62	88.45	38.03	16.27	45.44	49.80	0.986
	9	61	M	4.28	21.01	16.48	58.46	31.84	6.57	34.54	38.56	0.990
	10	59	M	7.76	23.62	42.46	6.26	2.76	1.09	21.61	36.72	0.980
	13	45	M	4.89	2.10	4.79	9.50	10.28	1.94	9.39	46.80	0.989
	14	42	M	7.19	4.14	25.54	17.01	15.66	5.78	22.02	45.03	0.994
	15	44	M	5.33	8.49	2.49	19.08	12.97	9.15	8.63	46.91	0.996
AT	1	45	M	6.35	4.92	34.00	24.60	17.07	4.57	35.36	35.05	0.996
	2	42	M	1.81	6.30	16.56	12.56	32.51	9.23	50.89	47.92	0.955
	3	56	M	0.28	13.90	116.87	17.37	23.05	12.65	66.32	37.93	0.993
	4	46	F	2.17	2.79	23.46	40.42	9.63	8.49	18.24	43.25	0.989
	5	46	M	9.59	1.30	4.21	19.03	32.30	6.98	13.39	54.96	0.994
	6	47	M	5.67	1.74	1.67	51.97	14.90	3.60	22.91	31.16	0.991
	7	48	F	12.22	10.28	42.43	36.55	12.54	11.36	26.27	42.98	0.995
	8	60	M	48.06	39.76	71.50	69.53	55.22	62.13	66.41	44.06	0.977
	9	61	M	37.61	52.07	125.25	19.36	33.20	76.95	79.94	31.33	0.943
	10	59	M	2.10	29.58	83.19	67.11	23.82	40.80	63.09	56.65	0.993
	11	67	M	26.77	105.78	60.56	9.80	28.12	53.78	88.23	41.14	0.951
	12	67	M	36.43	76.33	85.31	68.98	35.43	32.86	70.96	56.03	0.975
	13	45	M	49.46	8.31	58.77	90.48	17.13	93.97	56.47	74.07	0.962
	14	42	M	1.48	30.30	81.76	22.69	21.78	20.45	70.85	35.61	0.997
	15	44	M	1.83	11.07	51.42	19.94	9.63	10.97	44.57	33.52	0.996
PT	1	45	M	3.35	2.78	24.25	24.02	16.73	5.73	15.08	43.84	0.995
	2	42	M	6.63	1.52	7.72	7.96	15.48	3.11	16.96	48.61	0.913
	3	56	M	3.66	6.56	60.82	27.69	13.04	11.03	36.68	41.87	0.984
	4	46	F	10.41	12.78	30.43	20.28	5.92	5.64	17.49	57.95	0.993
	5	46	M	13.07	6.09	8.81	7.65	10.14	2.86	16.03	42.16	0.993
	6	47	M	3.89	6.82	1.10	9.32	9.68	4.62	7.07	57.42	0.979

Location	No	Age, years	Sex	C_{gr}, kPa	C_1^{el}, kPa	C_2^{el}	C_1^{smc}, kPa	$C2smc$	C_1^{col}, kPa	C_2^{col}	γ, deg	R^2
	7	48	F	8.73	0.55	38.46	50.47	21.45	10.02	26.06	37.55	0.993
	8	60	M	37.17	66.03	84.11	66.04	29.85	56.68	84.32	35.51	0.986
	9	61	M	55.41	17.80	61.78	81.99	39.94	65.12	77.62	57.54	0.969
	10	59	M	5.24	14.83	43.45	46.40	11.93	14.46	33.96	39.75	0.998
	11	67	M	19.55	68.69	112.75	20.70	29.27	52.87	84.84	37.55	0.991
	12	67	M	3.45	96.45	92.98	35.58	23.28	48.51	70.98	38.61	0.989
	15	44	M	3.80	17.53	60.30	29.17	11.85	14.08	30.27	38.37	0.997
FA	1	45	M	5.17	1.84	19.13	19.18	11.83	4.16	18.92	39.71	0.994
	2	42	M	0.60	3.64	17.65	40.95	42.20	11.99	35.31	46.46	0.963
	3	56	M	6.31	20.64	57.30	33.27	8.72	8.66	32.74	42.86	0.992
	4	46	F	10.47	1.71	24.10	49.75	13.97	7.12	23.32	47.10	0.993
	5	46	M	12.69	12.27	21.94	15.64	11.49	0.69	30.79	41.02	0.989
	6	47	M	5.79	6.90	14.54	20.61	6.43	3.47	24.69	34.19	0.990
	7	48	F	7.10	1.80	35.88	46.84	22.84	8.49	34.01	40.98	0.993
	8	60	M	28.69	28.10	54.44	81.58	18.88	54.44	36.65	40.83	0.985
	9	61	M	1.63	46.46	92.12	82.31	21.39	41.83	83.39	33.66	0.986
	10	59	M	0.03	38.15	78.93	69.36	17.81	16.36	62.16	42.85	0.992
	11	67	M	0.10	23.37	55.57	35.82	11.60	25.24	47.73	34.77	0.995
	12	67	M	51.77	2.20	56.36	86.98	13.19	65.75	28.45	73.31	0.942
	14	42	M	0.13	9.98	30.72	77.70	62.64	52.50	57.82	37.29	0.932
	15	44	M	9.94	8.79	22.41	49.59	19.20	4.25	28.80	46.71	0.994

Data availability

Data will be made available from the corresponding author upon a reasonable request.

References

[1]. Mahoney EM, Wang K, Keo HH, Duval S, Smolderen KG, Cohen DJ, Steg G, Bhatt DL, Hirsch AT, Vascular hospitalization rates and costs in patients with peripheral artery disease in the United States, Circ. Cardiovasc. Qual. Outcomes 3 (2010) 642–651, doi:10.1161/CIRCOUTCOMES.109.930735. [PubMed: 20940249]

[2]. Watt JKJ, Origin of femoro-popliteal occlusions, Br. Med. J 2 (1965) 1455–1459, doi:10.1136/bmj.2.5476.1455. [PubMed: 5849435]

[3]. Narula N, Dannenberg AJ, Olin JW, Bhatt DL, Johnson KW, Nadkarni G, Min J, Torii S, Poojary P, Anand SS, Bax JJ, Yusuf S, Virmani R, Narula J, Pathology of peripheral artery disease in patients with critical limb ischemia, J. Am. Coll. Cardiol 72 (2018) 2152–2163, doi:10.1016/j.jacc.2018.08.002. [PubMed: 30166084]

[4]. Mahoney EM, Wang K, Cohen DJ, Hirsch AT, Alberts MJ, Eagle K, Mosse F, Jackson JD, Steg PG, Bhatt DL, One-year costs in patients with a history of or at risk for atherothrombosis in the United States, Circ. Cardiovasc. Qual. Outcomes 1 (2008) 38–45, doi:10.1161/CIRCOUTCOMES.108.775247. [PubMed: 20031786]

[5]. Scully RE, Arnaoutakis DJ, DeBord Smith A, Semel M, Nguyen LL, Estimated annual health care expenditures in individuals with peripheral arterial disease, J. Vasc. Surg 67 (2018) 558–567, doi:10.1016/J.JVS.2017.06.102. [PubMed: 28847660]

[6]. Adam DJ, Beard JD, Cleveland T, Bell J, Bradbury aW., Forbes JF, Fowkes FGR, Gillepsie I, Ruckley CV, Raab G, Storkey H, Bypass versus angioplasty in severe ischaemia of the leg (BASIL): multicentre, randomised controlled trial, Lancet 366 (2005) 1925–1934, doi:10.1016/S0140-6736(05)67704-5. [PubMed: 16325694]

[7]. Conte MS, Bandyk DF, Clowes AW, Moneta GL, Seely L, Lorenz TJ, Namini H, Hamdan AD, Roddy SP, Belkin M, Berceli S.a., DeMasi RJ, Samson RH, Berman SS, Results of PREVENT III: a multicenter, randomized trial of edifoligide for the prevention of vein graft failure in lower extremity bypass surgery, J. Vasc. Surg 43 (2006) 742–751, doi:10.1016/j.jvs.2005.12.058. [PubMed: 16616230]

[8]. Schillinger M, Sabeti S, Loewe C, Dick P, Amighi J, Mlekusch W, Schlager O, Cejna M, Lammer J, Minar E, Balloon angioplasty versus implantation of nitinol stents in the superficial femoral artery, N. Engl. J. Med 354 (2006) 1879–1888, doi:10.1056/NEJMoa051303. [PubMed: 16672699]

[9]. Schillinger M, Sabeti S, Dick P, Amighi J, Mlekusch W, Schlager O, Loewe C, Cejna M, Lammer J, Minar E, Sustained benefit at 2 years of primary femoropopliteal stenting compared with balloon angioplasty with optional stenting, Circulation 115 (2007) 2745–2749, doi:10.1161/CIRCULATIONAHA.107.688341. [PubMed: 17502568]

[10]. Stavroulakis K, Torsello G, Manal A, Schwindt A, Hericks C, Stachmann A, Schönefeld E, Bisdas T, Results of primary stent therapy for femoropopliteal peripheral arterial disease at 7 years, J. Vasc. Surg 64 (2016) 1696–1702, doi:10.1016/j.jvs.2016.05.073. [PubMed: 27575816]

[11]. Laird JR, Yeo KK, The Treatment of Femoropopliteal In-Stent Restenosis Back to the Future*, 2012, doi:10.1016/j.jacc.2011.09.037.

[12]. Qato K, Conway AM, Mondry L, Giangola G, Carroccio A, Management of isolated femoropopliteal in-stent restenosis, J. Vasc. Surg 68 (2018) 807–810, doi:10.1016/j.jvs.2018.01.030. [PubMed: 30144908]

[13]. Lundgren F, External support of a polytetrafluoroethylene graft improves patency for bypass to below-knee arteries, Ann. Vasc. Surg 27 (2013) 1124–1133, doi:10.1016/j.avsg.2013.02.009. [PubMed: 23972437]

[14]. Albertini JN, Barral X, Branchereau A, Favre JP, Guidicelli H, Magne JL, Magnan PE, Long-term results of arterial allograft below-knee bypass grafts for limb salvage: a retrospective multicenter study, J. Vasc. Surg 31 (2000) 426–435, doi:10.1067/mva.2000.103792. [PubMed: 10709053]

[15]. Mustapha JA, Finton SM, Diaz-Sandoval LJ, Saab FA, Miller LE, Percutaneous transluminal angioplasty in patients with infrapopliteal arterial disease, Circ. Cardiovasc. Interv 9 (2016) 1–10, doi:10.1161/CIRCINTERVENTIONS.115.003468.

[16]. Teichgräber U, Lehmann T, Thieme M, Wahl KU, Stelzner C, Bormann A, Göotz L, Kroeßner T, Boden H, Maiwald L, Aschenbach R, Drug-coated balloon angioplasty of infrapopliteal lesions in patients with critical limb ischaemia: 1-year results of the APOLLO trial, Cardiovasc. Intervent. Radiol 42 (2019) 1380–1390, doi:10.1007/s00270-019-02279-6. [PubMed: 31286197]

[17]. Giles KA, Pomposelli FB, Hamdan AD, Blattman SB, Panossian H, Schermerhorn ML, Infrapopliteal angioplasty for critical limb ischemia: relation of TransAtlantic InterSociety Consensus class to outcome in 176 limbs, J. Vasc. Surg 48 (2008) 128–136, doi:10.1016/j.jvs.2008.02.027. [PubMed: 18502084]

[18]. Christenson BM, Rochon P, Gipson M, Gupta R, Smith MT, Treatment of infrapopliteal arterial occlusive disease in critical limb ischemia, Semin. Interv. Radiol 31 (2014) 370–374, doi:10.1055/s-0034-1393974.

[19]. Humphrey JD, Dufresne ER, Schwartz M.a., Mechanotransduction and extracellular matrix homeostasis, Nat. Rev. Mol. Cell Biol 15 (2014) 802–812, doi:10.1038/nrm3896. [PubMed: 25355505]

[20]. Kamenskiy A, Seas A, Bowen G, Deegan P, Desyatova A, Bohlim N, Poulson W, Mactaggart J, In situ longitudinal pre-stretch in the human femoropopliteal artery, Acta Biomater. 32 (2016) 231–237, doi:10.1016/j.actbio.2016.01.002. [PubMed: 26766633]

[21]. Jadidi M, Razian SA, Anttila E, Doan T, Adamson J, Pipinos M, Kamenskiy A, Comparison of morphometric, structural, mechanical, and physiologic characteristics of human

superficial femoral and popliteal arteries, Acta Biomater. 121 (2021) 431–443, doi:10.1016/j.actbio.2020.11.025. [PubMed: 33227490]

[22]. Kamenskiy A, Poulson W, Sim S, Reilly A, Luo J, Mactaggart J, Prevalence of calcification in human femoropopliteal arteries and its association with demographics, risk factors, and arterial stiffness, Arterioscler. Thromb. Vasc. Biol 38 (2018) ATVBAHA.117.310490, doi:10.1161/ATVBAHA.117.310490.

[23]. Jadidi M, Desyatova A, MacTaggart J, Kamenskiy A, Mechanical stresses associated with flattening of human femoropopliteal artery specimens during planar biaxial testing and their effects on the calculated physiologic stress-stretch state, Biomech. Model. Mechanobiol 18 (2019) 1591–1605, doi:10.1007/s10237-019-01162-0. [PubMed: 31069592]

[24]. Kamenskiy A, Seas A, Deegan P, Poulson W, Anttila E, Sim S, Desyatova A, MacTaggart J, Constitutive description of human femoropopliteal artery aging, Biomech. Model. Mechanobiol 16 (2017) 681–692, doi:10.1007/s10237-016-0845-7. [PubMed: 27771811]

[25]. Kamenskiy AV, Pipinos II, Dzenis YA, Phillips NY, Desyatova AS, Kitson J, Bowen R, MacTaggart JN, Effects of age on the physiological and mechanical characteristics of human femoropopliteal arteries, Acta Biomater. 11 (2015) 304–313, doi:10.1016/j.actbio.2014.09.050. [PubMed: 25301303]

[26]. Anttila E, Balzani D, Desyatova A, Deegan P, MacTaggart J, Kamenskiy A, Mechanical damage characterization in human femoropopliteal arteries of different ages, Acta Biomater. 90 (2019) 225–240, doi:10.1016/j.actbio.2019.03.053. [PubMed: 30928732]

[27]. Desyatova A, MacTaggart J, Kamenskiy A, Constitutive modeling of human femoropopliteal artery biaxial stiffening due to aging and diabetes, Acta Biomater. 64 (2017) 50–58, doi:10.1016/j.actbio.2017.09.042. [PubMed: 28974476]

[28]. Jadidi M, Razian SA, Habibnezhad M, Anttila E, Kamenskiy A, Mechanical, structural, and physiologic differences in human elastic and muscular arteries of different ages: comparison of the descending thoracic aorta to the superficial femoral artery, Acta Biomater. 119 (2021) 268–283, doi:10.1016/j.actbio.2020.10.035. [PubMed: 33127484]

[29]. Carew TE, Vaishnav RN, Patel DJ, Compressibility of the Arterial Wall, Circ. Res 23 (1968) 61–68, doi:10.1161/01.RES.23.1.61. [PubMed: 5661939]

[30]. Jadidi M, Habibnezhad M, Anttila E, Maleckis K, Desyatova A, MacTaggart J, Kamenskiy A, Mechanical and structural changes in human thoracic aortas with age, Acta Biomater. 103 (2020) 172–188, doi:10.1016/j.actbio.2019.12.024. [PubMed: 31877371]

[31]. Storn R, Price K, Differential evolution – a simple and efficient heuristic for global optimization over continuous spaces, J. Glob. Optim 11 (1997) 341–359, doi:10.1023/A:1008202821328.

[32]. Humphrey JD, Eberth JF, Dye WW, Gleason RL, Fundamental role of axial stress in compensatory adaptations by arteries, J. Biomech 42 (2009) 1–8, doi:10.1016/j.jbiomech.2008.11.011. [PubMed: 19070860]

[33]. Razian SA, Jadidi M, Histology Image Viewer and Converter (HIVC): a high-speed freeware software to view and convert whole slide histology images, Comput. Methods Biomech. Biomed. Eng. Imaging Vis (2023) Accepted.

[34]. Eid MA, Mehta K, Barnes JA, Wanken Z, Columbo J, Stone DH, Goodney PP, Smith MM, Global burden of disease of peripheral artery disease, J. Vasc. Surg 74 (2021) e327, doi:10.1016/j.jvs.2021.07.078.

[35]. St. Hilaire C, Medial arterial calcification: a significant and independent contributor of peripheral artery disease, Arterioscler. Thromb. Vasc. Biol 42 (2022) 253–260, doi:10.1161/ATVBAHA.121.316252. [PubMed: 35081727]

[36]. Aday AW, Matsushita K, Epidemiology of peripheral artery disease and polyvascular disease, Circ. Res 128 (2021) 1818–1832, doi:10.1161/CIRCRESAHA.121.318535. [PubMed: 34110907]

[37]. Criqui MH, Aboyans V, Epidemiology of peripheral artery disease, Circ. Res 116 (2015) 1509–1526, doi:10.1161/CIRCRESAHA.116.303849. [PubMed: 25908725]

[38]. Soyoye DO, Abiodun OO, Ikem RT, Kolawole BA, Akintomide AO, Diabetes and peripheral artery disease: a review, World J. Diabetes 12 (2021) 827–838, doi:10.4239/wjd.v12.i6.827. [PubMed: 34168731]

[39]. Behrooz L, Abumoawad A, Rizvi SHM, Hamburg NM, A modern day perspective on smoking in peripheral artery disease, Front. Cardiovasc. Med 10 (2023) 1154708, doi:10.3389/fcvm.2023.1154708. [PubMed: 37187787]

[40]. Wang W, Zhao T, Geng K, Yuan G, Chen Y, Xu Y, Smoking and the pathophysiology of peripheral artery disease, Front. Cardiovasc. Med 8 (2021) 704106, doi:10.3389/fcvm.2021.704106. [PubMed: 34513948]

[41]. Aday AW, Everett BM, Dyslipidemia profiles in patients with peripheral artery disease, Curr. Cardiol. Rep 21 (2019) 42, doi:10.1007/s11886-019-1129-5. [PubMed: 31011836]

[42]. Tsai S, Vega GL, Coronary and peripheral artery plaques: do differences in plaque characteristics translate to differences in lipid management? J. Investig. Med 68 (2020) 1141–1151, doi:10.1136/jim-2019-001252.

[43]. Gupta A, Patel RAG, Peripheral arterial disease and hypertension, Curr. Opin. Cardiol 37 (2022) 403, doi:10.1097/HCO.0000000000000983. [PubMed: 35880444]

[44]. Itoga NK, Tawfik DS, Lee CK, Maruyama S, Leeper NJ, Chang TI, Association of blood pressure measurements with peripheral arterial disease events: a reanalysis of the ALLHAT data, Circulation 138 (2018) 1805–1814, doi:10.1161/CIRCULATIONAHA.118.033348. [PubMed: 29930023]

[45]. Cameron JD, Bulpitt CJ, Pinto ES, Rajkumar C, The aging of elastic and muscular arteries: a comparison of diabetic and nondiabetic subjects, Diabetes Care 26 (2003) 2133–2138, doi:10.2337/diacare.26.7.2133. [PubMed: 12832325]

[46]. Wang Y, Zeinali-Davarani S, Davis EC, Zhang Y, Effect of glucose on the biomechanical function of arterial elastin, J. Mech. Behav. Biomed. Mater 49 (2015) 244–254, doi:10.1016/j.jmbbm.2015.04.025. [PubMed: 26042769]

[47]. Wiemer M, Butz T, Schmidt W, Schmitz KP, Horstkotte D, Langer C, Scanning electron microscopic analysis of different drug eluting stents after failed implantation: from nearly undamaged to major damaged polymers, Catheter. Cardiovasc. Interv 75 (2010) 905–911, doi:10.1002/ccd.22347. [PubMed: 20088011]

[48]. Huang C-LL, Wu I-HH, Wu Y-WW, Hwang J-JJ, Wang S-SS, Chen W-JJ, Lee W-JJ, Yang W-SS, Association of lower extremity arterial calcification with amputation and mortality in patients with symptomatic peripheral artery disease, PLoS ONE 9 (2014) e90201, doi:10.1371/journal.pone.0090201. [PubMed: 24587279]

[49]. Randhawa MS, Reed GW, Grafmiller K, Gornik HL, Shishehbor MH, Prevalence of tibial artery and pedal arch patency by angiography in patients with critical limb ischemia and noncompressible ankle brachial index, Circ. Cardiovasc. Interv 10 (2017) 3–8, doi:10.1161/CIRCINTERVENTIONS.116.004605.

[50]. Lorbeer R, Grotz A, Dörr M, Völzke H, Lieb W, Kühn J-P, Mensel B, Reference values of vessel diameters, stenosis prevalence, and arterial variations of the lower limb arteries in a male population sample using contrast-enhanced MR angiography, PLoS ONE 13 (2018) e0197559, doi:10.1371/journal.pone.0197559. [PubMed: 29924802]

[51]. Ferrier TM, Comparative study of arterial disease in amputated lower limbs from diabetics and non-diabetics (with special reference to feet arteries), Med. J. Aust 1 (1967) 5–11. [PubMed: 5182855]

[52]. Ramdass M, Harnarayan P, Mooteeram N, Nath A, Naraynsingh V, Budhooram S, Dookie T, Henry R, Patterns of arteriosclerotic lesions of the lower extremity in a West Indian population based on angiographic findings and ethnicity, Ann. R. Coll. Surg. Engl 96 (2014) 121–126, doi:10.1308/003588414x13814021676756. [PubMed: 24780669]

[53]. Ansari F, Pack LK, Brooks SS, Morrison TM, Design considerations for studies of the biomechanical environment of the femoropopliteal arteries, J. Vasc. Surg 58 (2013) 804–813, doi:10.1016/j.jvs.2013.03.052. [PubMed: 23870198]

[54]. MacTaggart JN, Phillips NY, Lomneth CS, Pipinos III, Bowen R, Timothy Baxter B, Johanning J, Matthew Longo G, Desyatova AS, Moulton MJ, Dzenis YA, Kamenskiy AV, Three-dimensional bending, torsion and axial compression of the femoropopliteal artery during limb flexion, J. Biomech 47 (2014) 2249–2256, doi:10.1016/j.jbiomech.2014.04.053. [PubMed: 24856888]

[55]. Poulson W, Kamenskiy A, Seas A, Deegan P, Lomneth C, MacTaggart J, Limb flexion-induced axial compression and bending in human femoropopliteal artery segments, J. Vasc. Surg 67 (2018) 607–613, doi:10.1016/j.jvs.2017.01.071. [PubMed: 28526560]

[56]. Desyatova A, Poulson W, Deegan P, Lomneth C, Seas A, Maleckis K, MacTaggart J, Kamenskiy A, Limb flexion-induced twist and associated intramural stresses in the human femoropopliteal artery, J. R. Soc. Interface 14 (2017) 20170025, doi:10.1098/rsif.2017.0025. [PubMed: 28330991]

[57]. Nichols O'R, Vlachopoulos, McDonald's Blood Flow in Arteries, 2011 http://scholar.google.com/scholar?hl=en&btnG=Search&q=intitle:No+Title#0 (Accessed 13 January 2015).

[58]. Silverthorn DU, Human Physiology: An Integrated Approach, Pearson, 2010 .

[59]. Pries AR, Secomb TW, Microvascular blood viscosity in vivo and the endothelial surface layer, Am. J. Physiol. Heart Circ. Physiol 289 (2005) H2657–H2664, doi:10.1152/ajpheart.00297.2005. [PubMed: 16040719]

[60]. Libby P, Ridker PM, Hansson GK, Progress and challenges in translating the biology of atherosclerosis, Nature 473 (2011) 317–325, doi:10.1038/nature10146. [PubMed: 21593864]

[61]. Davies P, Flow-mediated endothelial mechanotransduction, Physiol. Rev 75 (1995) 519–560. [PubMed: 7624393]

[62]. Malek AM, Alper SL, Izumo S, Hemodynamics shear stress and its role in atherosclerosis, JAMA 282 (21) (1999) 2035–2042. [PubMed: 10591386]

[63]. Chatzizisis YS, Coskun AU, Jonas M, Edelman ER, Feldman CL, Stone PH, Role of endothelial shear stress in the natural history of coronary atherosclerosis and vascular remodeling: molecular, cellular, and vascular behavior, J Am Coll Cardiol 49 (2007) 2379–2393. [PubMed: 17599600]

[64]. Kamenskiy AV, Pipinos II, Dzenis YA, Lomneth CS, Kazmi SAJ, Phillips NY, MacTaggart JN, Passive biaxial mechanical properties and in vivo axial pre-stretch of the diseased human femoropopliteal and tibial arteries, Acta Biomater. 10 (2014) 1301–1313, doi:10.1016/j.actbio.2013.12.027. [PubMed: 24370640]

[65]. Kamenskiy AV, Pipinos II, Dzenis YA, Lomneth CS, Kazmi S. a J., Phillips NY, MacTaggart JN Passive biaxial mechanical properties and in vivo axial pre-stretch of the diseased human femoropopliteal and tibial arteries, Acta Biomater. 10 (2014) 1301–1313, doi:10.1016/j.actbio.2013.12.027. [PubMed: 24370640]

[66]. Shapiro SD, Endicott SK, Province MA, Pierce JA, Campbell EJ, Marked longevity of human lung parenchymal elastic fibers deduced from prevalence of D-aspartate and nuclear weapons-related radiocarbon, J. Clin. Invest 87 (1991) 1828–1834, doi:10.1172/JCI115204. [PubMed: 2022748]

[67]. Wells SM, Langille BL, Lee JM, Adamson SL, Determinants of mechanical properties in the developing ovine thoracic aorta, Am. J. Physiol 277 (1999) 1385–1391, doi:10.1152/ajpheart.1999.277.4.h1385.

[68]. Langille BL, Bendeck MP, Keeley FW, Adaptations of carotid arteries of young and mature rabbits to reduced carotid blood flow, Am. J. Physiol 256 (1989), doi:10.1152/ajpheart.1989.256.4.h931.

[69]. Bendeck MP, Langille BL, Rapid accumulation of elastin and collagen in the aortas of sheep in the immediate perinatal period, Circ. Res 69 (1991) 1165–1169, doi:10.1161/01.RES.69.4.1165. [PubMed: 1934343]

[70]. Davidson JM, Hill KE, Alford JL, Developmental changes in collagen and elastin biosynthesis in the porcine aorta, Dev. Biol 118 (1986) 103–111, doi:10.1016/0012-1606(86)90077-1. [PubMed: 3770292]

[71]. Fukuda Y, Ferrans VJ, Crystal RG, Development of elastic fibers of nuchal ligament, aorta, and lung of fetal and postnatal sheep: an ultrastructural and electron microscopic immunohistochemical study, Am. J. Anat 170 (1984) 597–629, doi:10.1002/AJA.1001700407. [PubMed: 6475819]

[72]. Nakamura H, Electron microscopic study of the prenatal development of the thoracic aorta in the rat, Am. J. Anat 181 (1988) 406–418, doi:10.1002/aja.1001810409. [PubMed: 3389308]

[73]. Mithieux SM, Weiss AS, Elastin, Adv. Protein Chem 70 (2005) 437–461, doi:10.1016/S0065-3233(05)70013-9. [PubMed: 15837523]

[74]. Jadidi M, Sherifova S, Sommer G, Kamenskiy A, Holzapfel GA, Constitutive modeling using structural information on collagen fiber direction and dispersion in human superficial femoral artery specimens of different ages, Acta Biomater. 121 (2021) 461–474, doi:10.1016/j.actbio.2020.11.046. [PubMed: 33279711]

[75]. Wight TN, A role for proteoglycans in vascular disease, Matrix Biol. J. Int. Soc. Matrix Biol 71–72 (2018) 396–420, doi:10.1016/j.matbio.2018.02.019.

[76]. Mattson JM, Turcotte R, Zhang Y, Glycosaminoglycans contribute to extracellular matrix fiber recruitment and arterial wall mechanics, Biomech. Model. Mechanobiol 16 (2017) 213–225, doi:10.1007/s10237-016-0811-4. [PubMed: 27491312]

[77]. Lepedda AJ, Nieddu G, Formato M, Baker MB, Fernández-Pérez J, Moroni L, Glycosaminoglycans: from vascular physiology to tissue engineering applications, Front. Chem 9 (2021) https://www.frontiersin.org/articles/10.3389/fchem.2021.680836. (Accessed 25 September 2023).

[78]. Zhang W, Jadidi M, Razian SA, Holzapfel G, Kamenskiy A, Nordsletten D, A viscoelastic constitutive model for human femoropopliteal arteries, Accept. 7 Sept. (2023).

[79]. Criqui MH, Vargas V, Denenberg JO, Ho E, Allison M, Langer RD, Gamst A, Bundens WP, Fronek A, Ethnicity and peripheral arterial disease: the San Diego population study, Circulation 112 (2005) 2703–2707, doi:10.1161/CIRCULATIONAHA.105.546507. [PubMed: 16246968]

[80]. Pabon M, Cheng S, Altin SE, Sethi SS, Nelson MD, Moreau KL, Hamburg N, Hess CN, Sex differences in peripheral artery disease, Circ. Res 130 (2022) 496–511, doi:10.1161/CIRCRESAHA.121.320702. [PubMed: 35175843]

[81]. Zhou B, Rachev A, Shazly T, The biaxial active mechanical properties of the porcine primary renal artery, J. Mech. Behav. Biomed. Mater (2015), doi:10.1016/j.jmbbm.2015.04.004.

Statement of significance

Peripheral Artery Disease (PAD) in the lower extremity arteries exhibits distinct characteristics and results in different clinical outcomes when treating arteries above and below the knee. However, their mechanical, structural, and physiologic differences are poorly understood. Our study compared above- and below-knee arteries from the same middle-aged human subjects and demonstrated distinct differences in size, structure, and mechanical properties, leading to variations in their physiological behavior. These insights could pave the way for creating location-specific medical devices and treatments for PAD, offering a more effective approach to its management. Our findings provide new, important perspectives for clinicians, researchers, and medical device developers interested in treating PAD in both above- and below-knee locations.

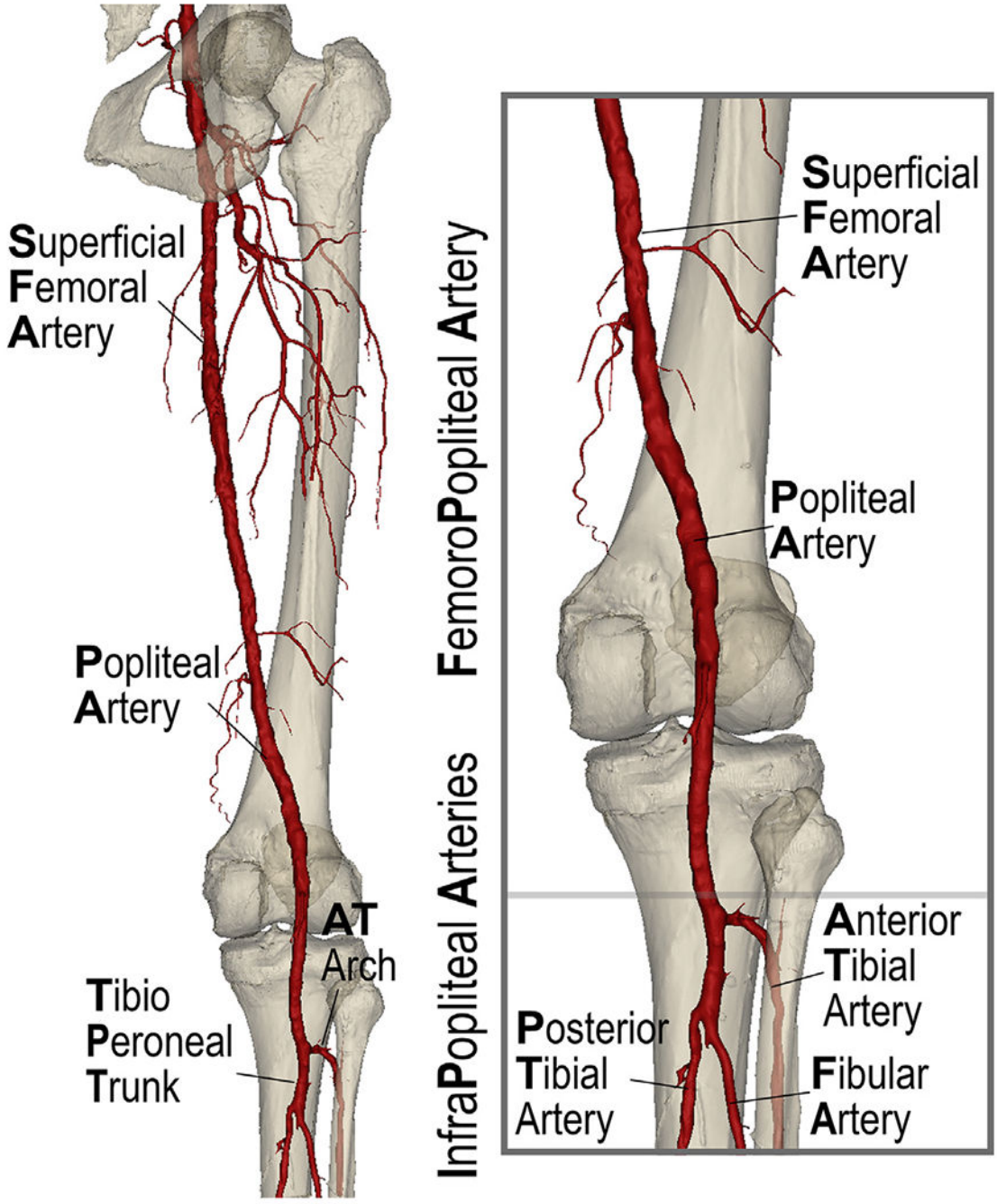

Fig. 1.

Arteries of the lower extremity include the superficial femoral (SFA) and the popliteal arteries (PA) that comprise the femoropopliteal (FPA) segment and the anterior tibial (AT), posterior tibial (PT), and fibular (peroneal) arteries (FA) that form the below-knee infrapopliteal (IPA) segment. The AT curves and develops an arch as it passes through the superior aspect of the interosseus membrane. Distal to the AT take-off, the PA continues as the tibioperoneal trunk (TPT) prior to bifurcating into the PT and FA.

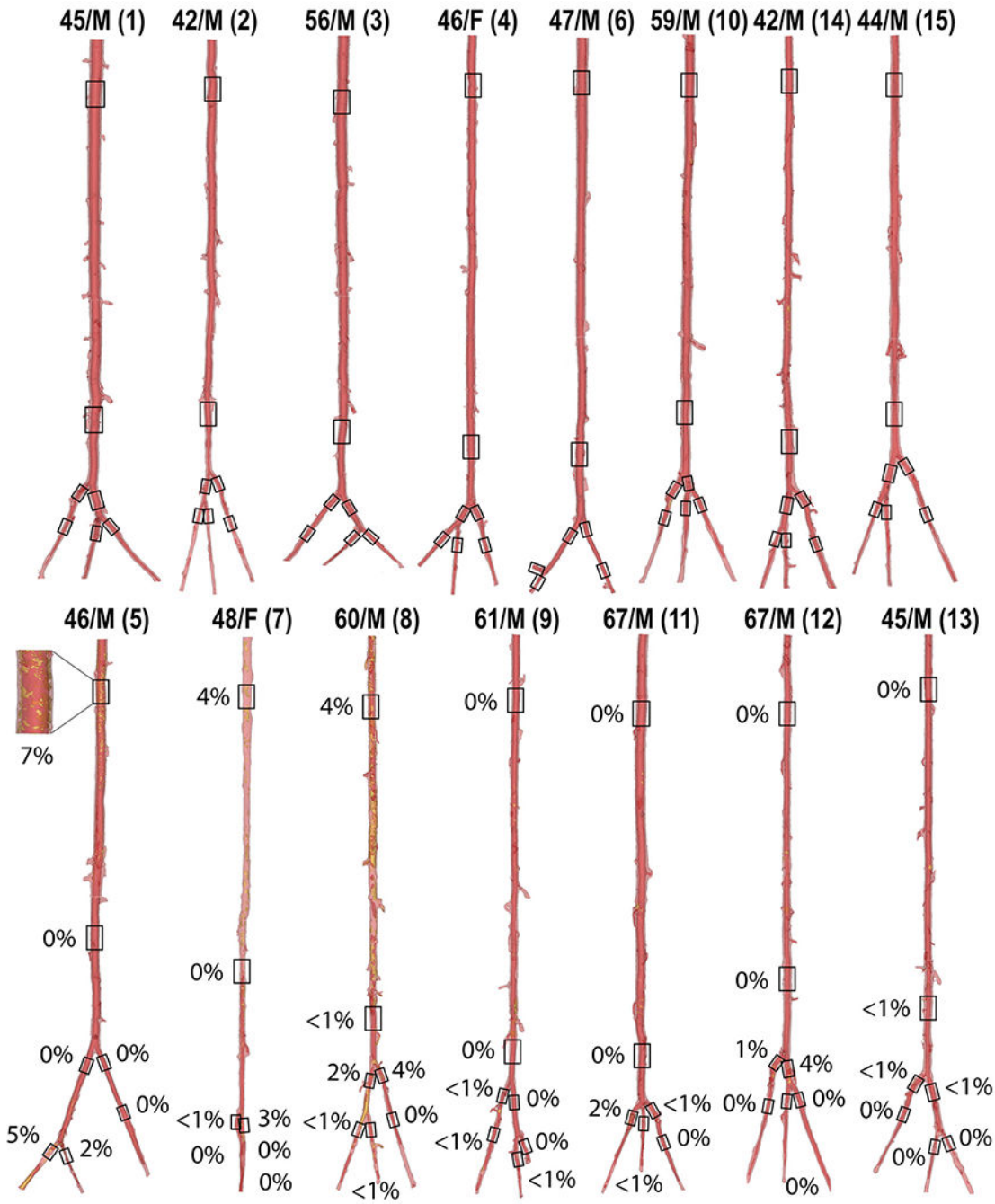

Fig. 2.

3D μCT reconstructions of all evaluated arteries. The top row represents vessels without calcification, while the bottom row depicts calcified arteries. The percentages indicate the amount of calcium present in each evaluated arterial segment, marked with a black box. The age and sex of each specimen are indicated at the top. Specimen numbers are in parentheses.

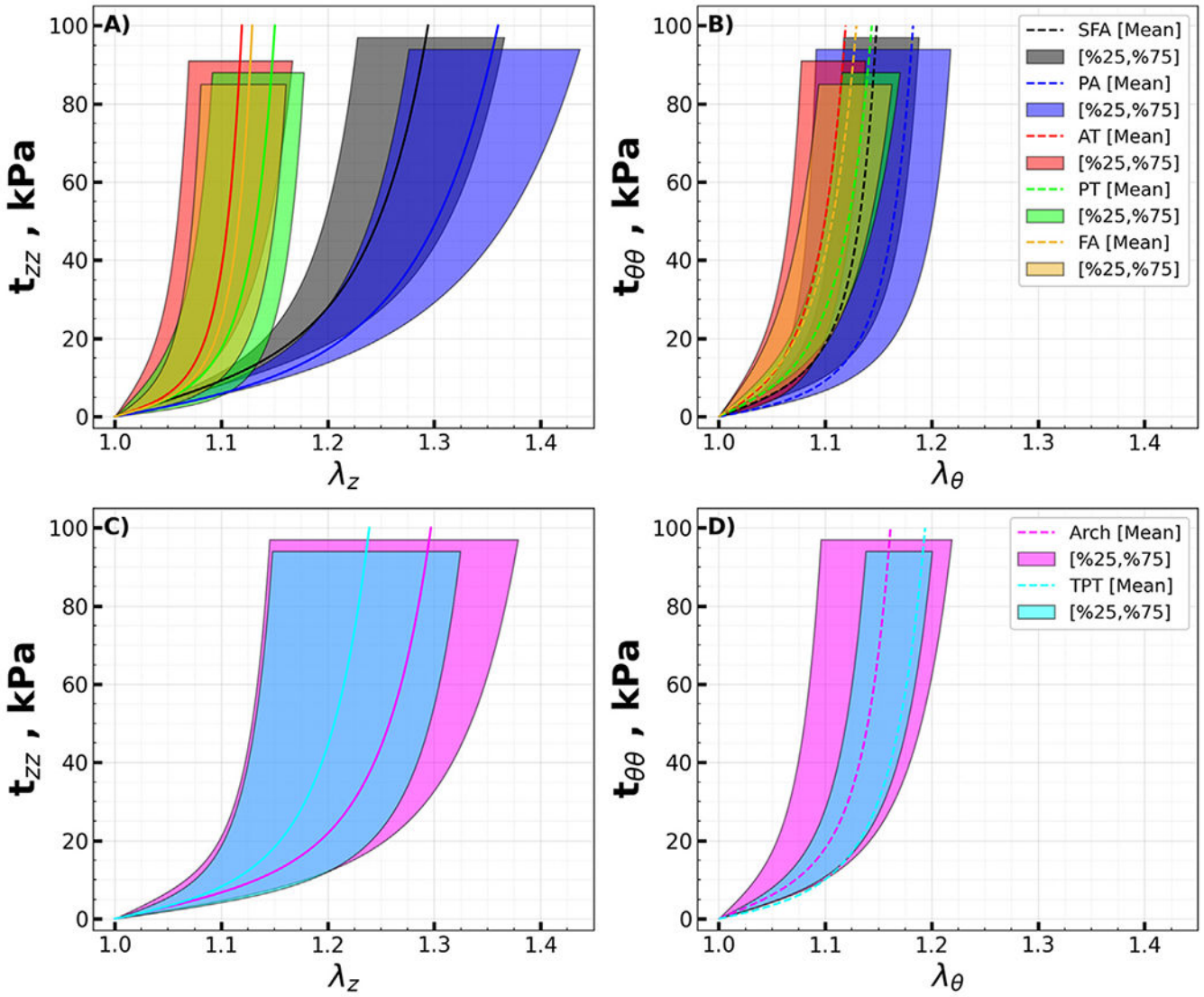

Fig. 3.

Mean equibiaxial Cauchy stress (kPa) - stretch curves for the A) above (SFA, PA) and B) below-knee (AT, PT, FA) arteries in longitudinal (solid lines, z) and circumferential (dashed lines, θ) directions. Transition zones (AT arch and TPT) are presented in panels C) and D). Variability is demonstrated by the shaded semi-transparent regions that bound 25th and 75th percentile ranges. They have different heights for better visualization.

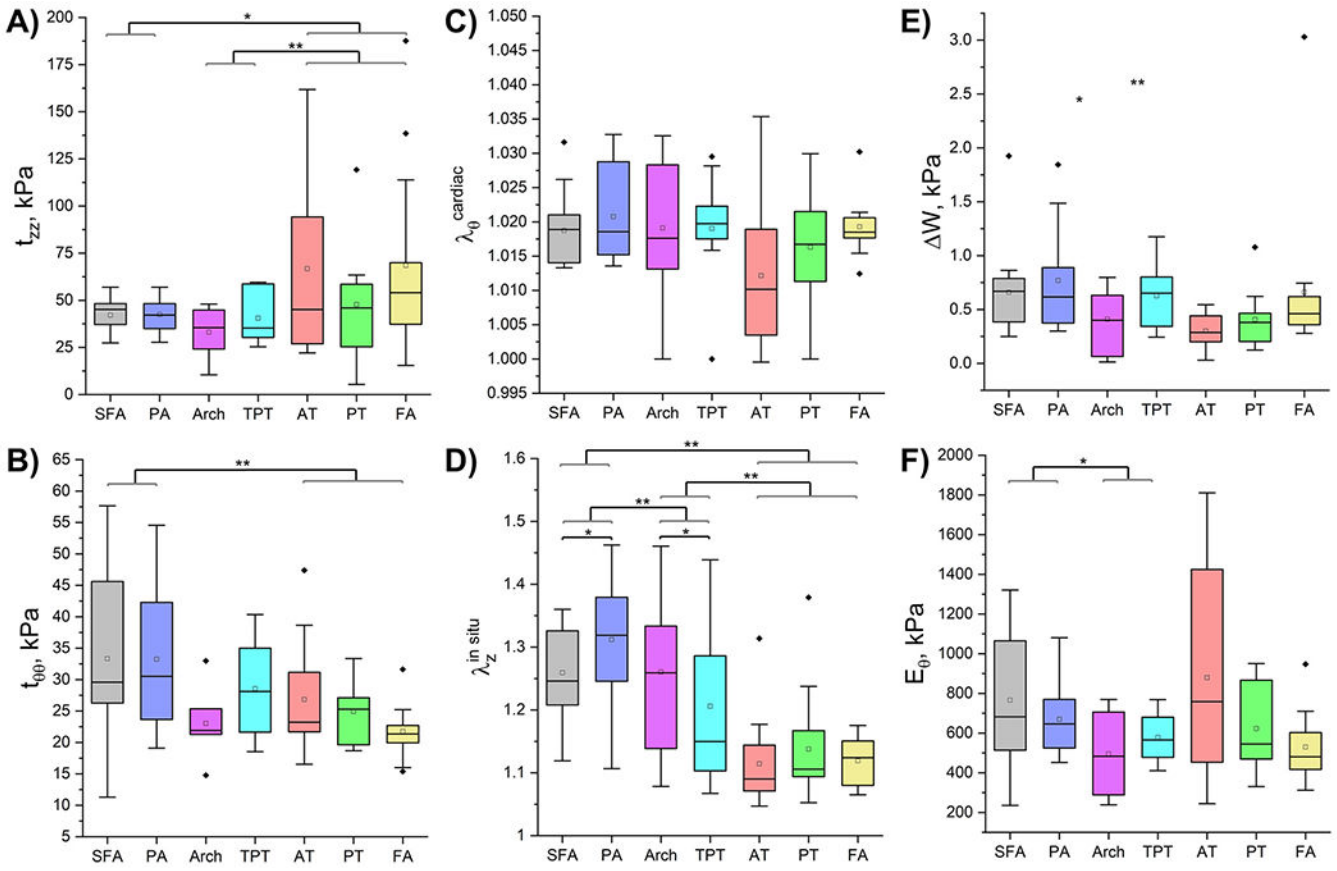

Fig. 4.

Calculated physiologic characteristics for all arterial segments demonstrating A) longitudinal and B) circumferential physiologic Cauchy stresses (kPa) at 100 mmHg pressure, C) circumferential cardiac cycle stretch as the artery deforms from diastole (80 mmHg) to systole (120 mmHg), D) *in situ* longitudinal pre-stretch, E) changes in stored elastic energy (kPa) over the cardiac cycle, and F) circumferential stiffness (kPa) defined as the change in circumferential physiologic stress divided by the change in the corresponding stretch during the cardiac cycle. Statistically significant differences between groups at $p < 0.05$ are marked with a single asterisk and at $p < 0.01$ with a double asterisk. The boxes bound 25th and 75th percentiles, mean values are marked with a hollow square, median is represented by a horizontal line within each box, and outliers are marked with a solid black rhombus. Whiskers extend to the outmost data point that falls within upper inner and lower inner fence defined by 75th percentile + 1.5x interquartile range and 25th percentile − 1.5x interquartile range, respectively.

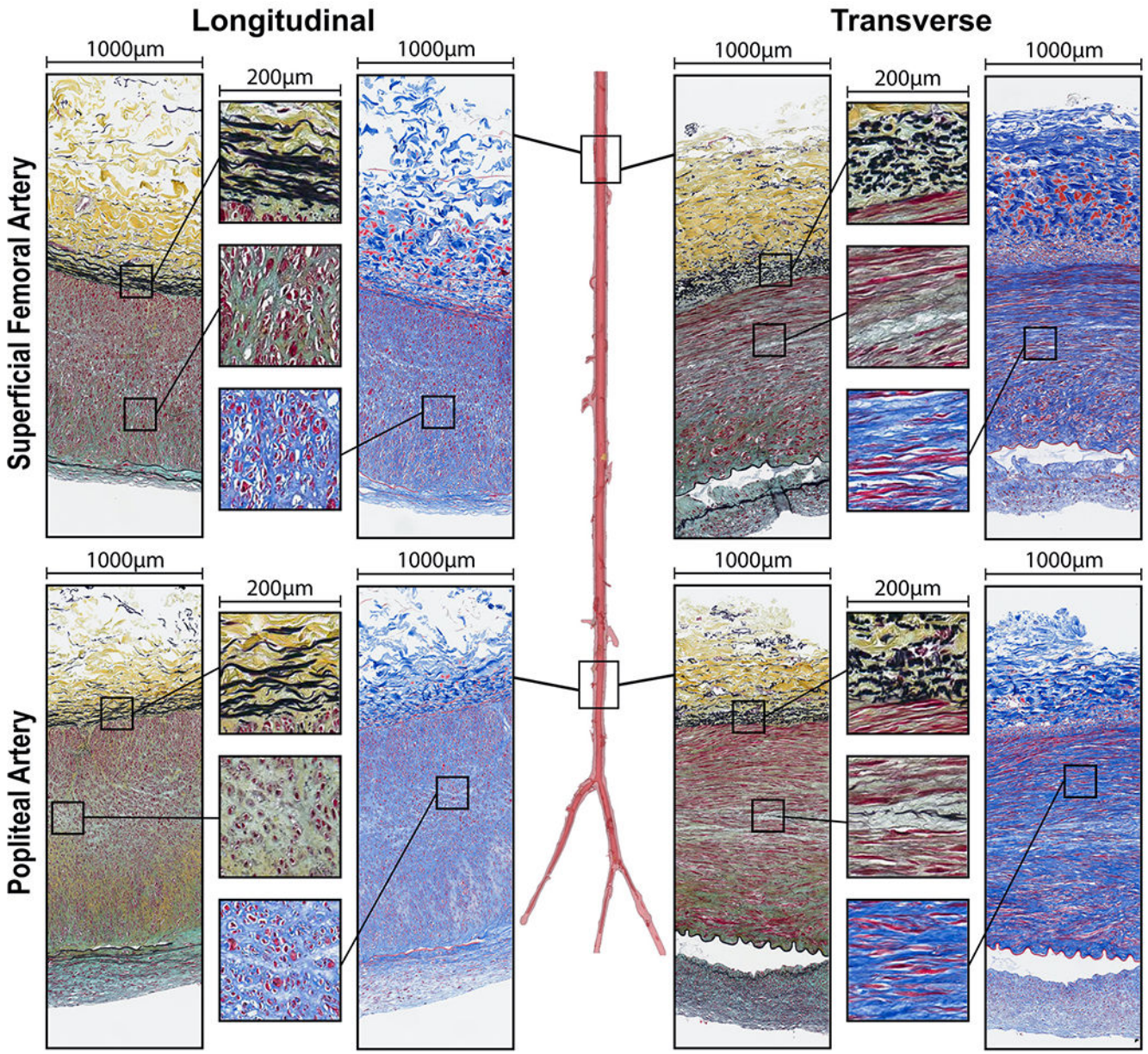

Fig. 5.

Structure of the superficial femoral (SFA) and popliteal (PA) arteries in longitudinal (left) and transverse (right) directions evaluated using Movat (elastin is black, glycosaminoglycans are greenish-gray) and Masson's Trichrome (collagen is blue, smooth muscle is red) stains. Note directional differences in elastin (longitudinal fibers) and SMCs (mostly circumferential) demonstrated by the inserts. Compare the structure of these above-knee arteries to the arteries below the knee from the same subject (Fig. 6).

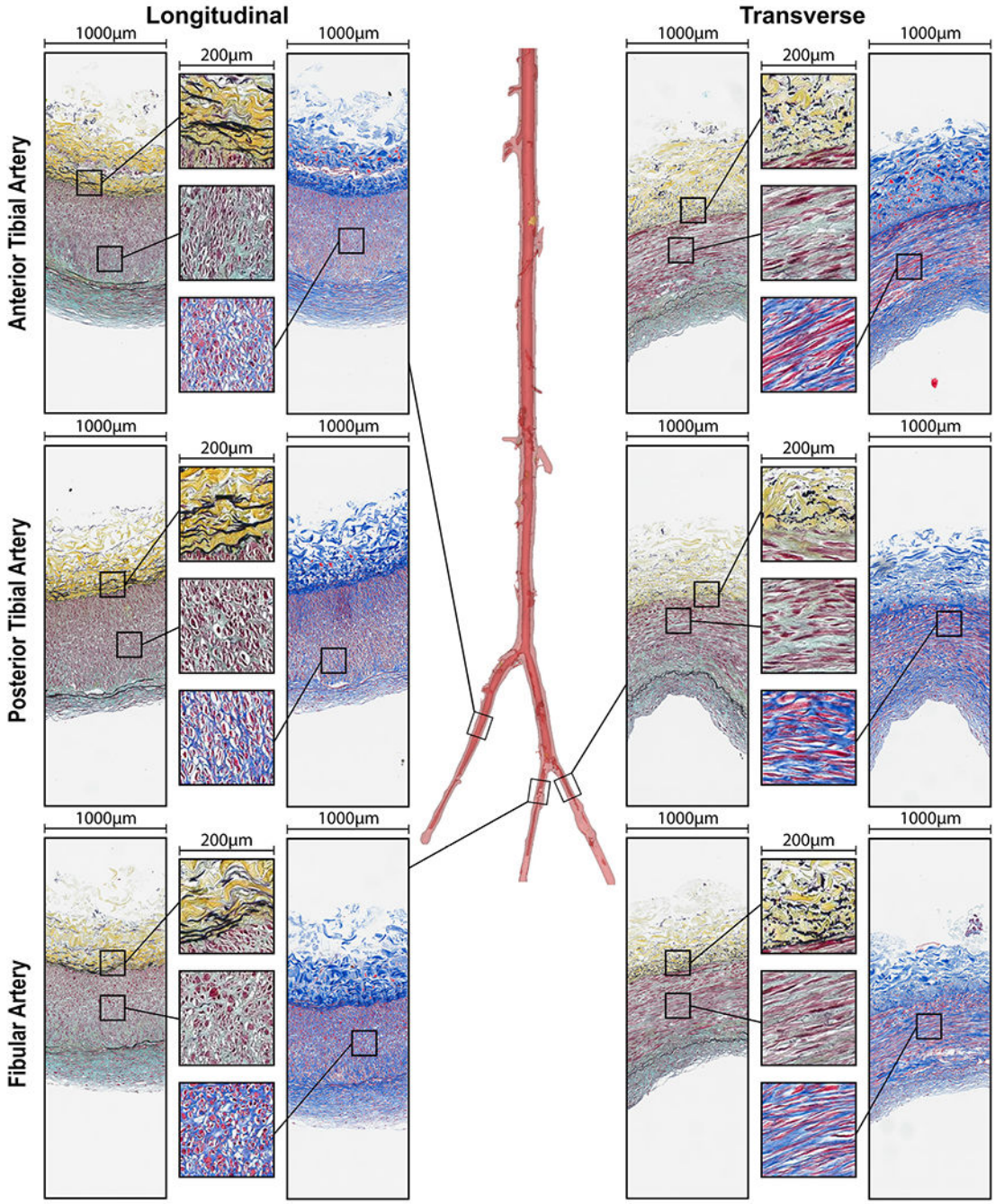

Fig. 6.

Structure of the anterior tibial (AT), posterior tibial (PT), and fibular (FA) arteries in longitudinal (left) and transverse (right) directions evaluated using Movat (elastin is black, glycosaminoglycans are greenish-gray) and Masson's Trichrome (collagen is blue, smooth muscle is red) stains. Note directional differences in elastin (longitudinal fibers) and medial SMCs (mostly circumferential) demonstrated by the inserts. Compare the structure of these below-knee arteries to the arteries above the knee from the same subject (Fig. 5).

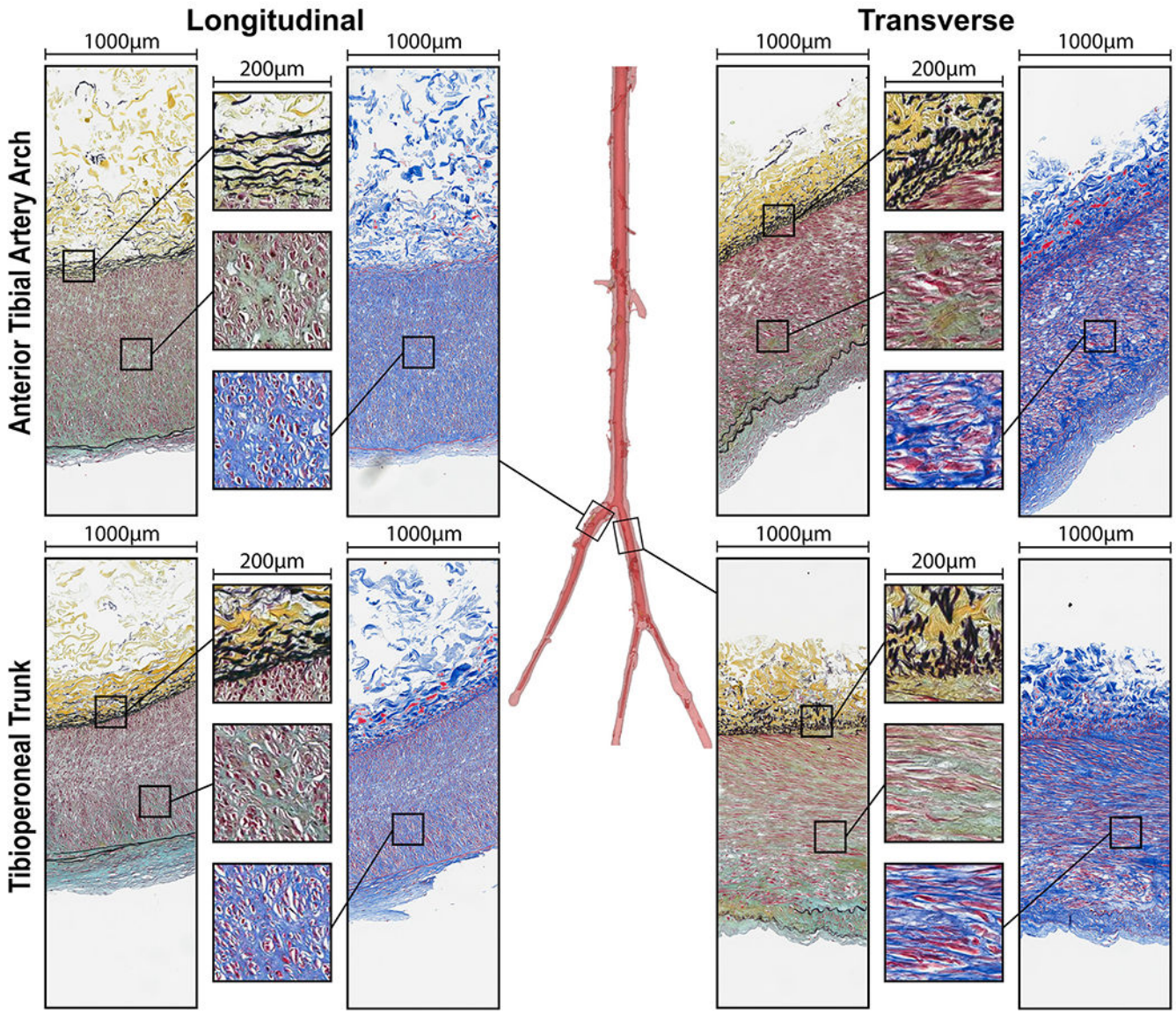

Fig. 7.

Structure of the transition zones: anterior tibial artery arch and the tibioperoneal trunk in longitudinal (left) and transverse (right) directions evaluated using Movat (elastin is black, glycosaminoglycans are greenish-gray) and Masson's Trichrome (collagen is blue, smooth muscle is red) stains. Note directional differences in elastin (longitudinal fibers) and medial SMCs (mostly circumferential) demonstrated by the inserts. Compare the structure of these transition zones to the arteries above (Fig. 5) and below (Fig. 6) the knee from the same subject.

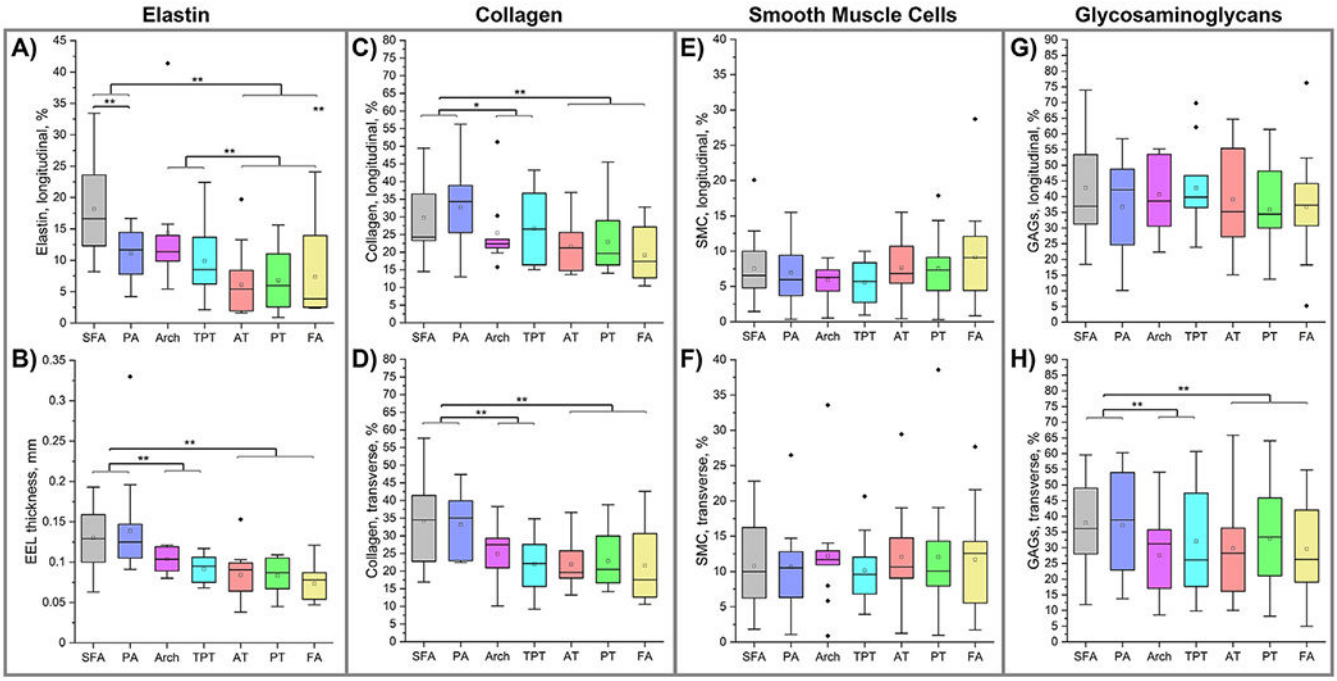

Fig. 8.

Structural composition of the above and below-knee arteries demonstrating the density of elastin in the EEL (A), thickness of the EEL (B), collagen content (C,D), smooth muscle cell (E,F), and glycosaminoglycan (G, H) content in the tunica media measured using longitudinal (top row) and circumferential (bottom row) sections. Statistically significant differences between groups at $p < 0.05$ are marked with a single asterisk and at $p < 0.01$ with a double asterisk. The boxes bound 25th and 75th percentiles, mean values are marked with a hollow square, median is represented by a horizontal line within each box, and outliers are marked with a solid black rhombus. Whiskers extend to the outmost data point that falls within upper inner and lower inner fence defined by 75th percentile + 1.5x interquartile range and 25th percentile − 1.5x interquartile range, respectively.

Table 1

Demographics and risk factors of all subjects in the study.

No	Age	Sex	BMI	HTM	DM	DLD	CAD	Smoking	Cause of death	Disease stage [20,21] SFA/PA/arch/TPT/AT/PT/FA
1	45	M	39.4	No	No	No	No	Former	MI	III/III/IV/III/IV/III/II
2	42	M	41.9	Yes	No	No	No	Never	Cardiac Arrest	II/I/II/III/IV/IV/III/II
3	56	M	33.9	Yes	No	No	Yes	Current	Cardiac Arrest	III/II/II/IV/III/III/III
4	46	F	23.2	No	No	No	No	Never	Cardiac Arrest	I/II/II/II/III/II/II
5	46	M	53.1	Yes	Yes	No	No	Never	Respiratory Failure	IV/II/III/IV/IV/III/IV
6	47	M	26.2	No	No	No	No	Current	GSW	I/II/III/II/II/I/II
7	48	F	28.4	Yes	Yes	Yes	No	Current	CVA/Stroke	IV/IV/II/III/II/II/II
8	60	M	23.1	Yes	No	Yes	Yes	Current	Cardiac Arrest	III/III/III/IV/IV/IV/III
9	61	M	23.7	Yes	No	No	No	Current	Cardiac Arrest	II/II/IV/II/III/III/III
10	59	M	43.1	Yes	No	Yes	No	Never	Cardiac Arrest	III/III/III/III/III/III/III
11	67	M	29.1	No	No	No	No	Current	Cardiac Arrest	III/III/III/NA/III/III/III
12	67	M	22.6	Yes	No	No	No	Current	Cardiac Arrest	III/II/III/IV/III/II/II
13	45	M	NA	No	No	No	No	Never	Respiratory Arrest	III/IV/III/III/III/III/III
14	42	M	NA	Yes	No	No	No	Current	Cardiac Arrest	III/III/III/III/III/II/II
15	44	M	32.7	No	No	No	No	Current	Cardiac Arrest	I/I/I/I/II/II/I

BMI = body mass index, HTN = hypertension, DM = diabetes mellitus, DLD = dyslipidemia, CAD = coronary artery disease, M = male, F = female, MI = myocardial infarction, GSW = gunshot wound, CVA = cerebrovascular accident, NA = data not available.

For the details of disease stage assessment please refer to Section 2.7 below or to our previous works [20–22].

Table 2

Inner diameters, wall thickness, and opening angles for different arterial segments.

	Inner diameter, mm	Thickness, load-free, mm	Thickness, stress-free, mm	Opening angle, transverse, °	Opening angle, longitudinal, °
SFA	5.60±2.41	1.83±0.25	1.91±0.35	211±71	190±68
PA	4.35±0.93	1.74±0.23	1.86±0.26	212±52	178±66
Arch	2.82±0.39	1.40±0.33	1.61±0.34	212±54	225±63
TPT	3.37±0.88	1.52±0.33	1.57±0.31	228±60	217±24
AT	2.51±0.49	1.22±0.24	1.29±0.18	232±55	161±88
PT	2.18±0.36	1.21±0.21	1.22±0.17	229±47	180±61
FA	2.05±0.42	1.08±0.16	1.16±0.16	202±53	179±68

Data are presented as average ± standard deviation.

SFA = Superficial Femoral Artery, PA = Popliteal Artery, Arch = arch of the Anterior Tibial (AT) artery, TPT = tibioperoneal trunk, PT = Posterior Tibial artery, FA = Fibular (peroneal) artery.

Table 3

Constitutive parameters for the four-fiber-family model describing the average specimens for each arterial location.

Location	C_{gr}(kPa)	C_1^{el}(kPa)	C_2^{el}	C_1^{smc}(kPa)	C_2^{smc}	C_1^{col}(kPa)	C_2^{col}	γ, deg	R^2
SFA	8.78	13.42	2.60	15.08	17.09	4.96	13.67	53.39	0.999
PA	2.47	12.86	1.38	9.26	11.28	6.31	7.88	55.49	0.999
Arch	7.31	8.29	3.57	18.45	11.25	5.23	12.08	53.40	0.999
TPT	2.90	15.15	5.10	15.15	9.85	5.37	10.58	45.84	0.999
AT	3.91	16.66	28.38	44.55	19.62	15.93	37.84	40.71	0.999
PT	5.45	13.76	19.04	28.99	14.86	11.10	23.96	43.81	0.999
FA	6.50	13.02	27.34	51.45	15.36	9.15	36.03	38.48	0.999

Table 4

Constitutive parameters for the four-fiber-family model describing the 25th percentile specimens for each arterial location.

Location	C_{gr}(kPa)	C_1^{el}(kPa)	C_2^{el}	C_1^{smc}(kPa)	C_2^{smc}	C_1^{col}(kPa)	C_2^{col}	γ, deg	R^2
SFA	12.29	14.73	6.06	24.78	22.44	2.69	33.65	56.15	0.996
PA	8.18	11.43	3.17	21.32	48.05	6.92	23.82	53.92	0.994
Arch	19.24	6.28	29.09	27.57	42.60	16.51	35.00	48.93	0.993
TPT	10.56	11.69	21.94	25.34	20.33	7.49	25.89	40.34	0.993
AT	34.21	69.22	61.20	62.51	28.23	24.27	100.20	49.54	0.987
PT	26.10	30.04	51.80	11.50	34.57	26.77	32.52	50.83	0.995
FA	8.12	27.63	53.16	94.01	18.69	39.95	53.66	38.08	0.990

Table 5

Constitutive parameters for the four-fiber-family model describing the 75th percentile specimens for each arterial location.

Location	C_{gr}(kPa)	C_1^{el}(kPa)	C_2^{el}	C_1^{smc}(kPa)	C_2^{smc}	C_1^{col}(kPa)	C_2^{col}	γ, deg	R^2
SFA	11.12	7.94	1.69	7.46	13.40	1.24	10.41	52.06	0.995
PA	4.22	11.95	0.64	9.67	6.96	2.02	6.87	56.65	0.997
Arch	5.52	5.86	1.84	16.40	6.93	1.96	5.51	43.19	0.987
TPT	6.02	3.82	3.85	15.45	7.89	1.49	10.17	48.32	0.991
AT	1.68	21.05	9.73	13.03	21.43	14.07	20.86	47.09	0.952
PT	4.83	2.36	25.19	20.00	8.88	10.40	14.17	52.84	0.976
FA	2.09	12.72	10.81	33.60	9.65	4.80	24.81	35.27	0.989